의학박사 학위논문

The functional role of succinate dehydrogenase in regulatory T cells

조절 T 세포에서 숙신산 탈수소효소의 기능

2023년 2월

서울대학교 대학원

의학과 병리학 전공

김 세 희

The functional role of succinate dehydrogenase in regulatory T cells

지도 교수 전 윤 경

이 논문을 의학박사 학위논문으로 제출함
2022년 10월

서울대학교 대학원
의학과 병리학 전공
김 세 희

김세희의 의학박사 학위논문을 인준함
2023년 1월

위 원 장 _____ (인)

부위원장 _____ (인)

위 원 _____ (인)

위 원 _____ (인)

위 원 _____ (인)

The functional role of succinate dehydrogenase in regulatory T cells

By Sehui Kim

(Directed by Professor Yoon Kyung Jeon, M.D., PhD)
A Thesis submitted to the Department of Medicine in partial fulfillment of the requirements for the Degree of Doctor of Philosophy (Pathology) in Medicine at Seoul National University

October 2022

Approved by Thesis Committee

January 2023

Professor_____(Seal) Chairperson

Professor_____(Seal) Vice Chairperson

Professor_____(Seal)

Professor_____(Seal)

Professor_____(Seal)

Abstract

The functional role of succinate dehydrogenase in regulatory T cells

김 세 희 (Sehui Kim)
의학과 (Department of Medicine)
병리학 전공 (Major in Pathology)
The Graduate School
Seoul National University

There is growing interest in the biology of regulatory T (Treg) cells because they are key regulators of peripheral tolerance and response to various immunotherapies. In the quest for a better understanding of the biology of Treg cells, the distinct metabolic programming of Treg cells has been widely studied, but there are still major unknowns in terms of their clinical impact and the application of modulating the metabolism of Treg cells in a tumor microenvironment (TME). Succinate dehydrogenase (SDH) is one of the key molecules involved in mitochondrial metabolism, which involves in both the tricarboxylic acid cycle (TCA) cycle and electron transfer chain (ETC). In this study, I disrupted mitochondrial metabolism by deletion of SDHA, a subunit of

SDH, and evaluated its role in Treg cell homeostasis and suppressive functions. I showed that deletion of SDHA in Treg cells resulted in impaired suppressive activity and triggered scurfy phenotypes. SDHA-deficient Treg cells showed proinflammatory cytokine secretion and diminished the transcriptional factor forkhead box P3 (FOXP3) expression. I found that this phenotype was partly due to increased glycolysis. In the mouse model employed, tumor development or growth was dampened by increased anti-tumor immunity. Similar to the SDHA-deficient Treg cells, a $FOXP3^{low}$ Treg cell subpopulation was identified, and they showed increased proinflammatory cytokine secretion in human tumor tissues. A high ratio of $FOXP3^{low}$ cells/$FOXP3^{+}$ cells in the TME was related to better overall survival in colon adenocarcinoma and lung squamous cell carcinoma being treated with conventional therapies. This tendency was also observed in lung squamous cell carcinoma patients undergoing PD-1/PD-L1 blockade therapy. In conclusion, SDHA is crucial for Treg cell maintenance and suppressive capacity, and evaluating the subpopulation of Treg cells is important for forecasting the survival of tumor patients.

Keywords: succinate dehydrogenase, mitochondrial metabolism, FOXP3, regulatory T cell, tumor

Student Number: 2014-30592

CONTENTS

LIST OF TABLES

LIST OF FIGURES

List of abbreviation

2-DG, 2-Deoxy-D-glycose

ADC, adenocarcinoma

DC, dendritic cell

ELISA, enzyme-linked immunosorbent assay

ETC, electron transport chain

FACS, fluorescence-activated Cell Sorting

FAO, fatty acid oxidation

FOXP3, Forkhead Box P3

HE, hematoxylin and eosin

HK2, hexokinase 2

IFN, interferon

IHC, immunohistochemistry

MDSC, myeloid-derived suppressor cell

MSS, microsatellite stable

NK cell, Natural killer cell

OXPHOS, oxidative phosphorylation

PMA, phorbol myristate acetate

qRT-PCR, quantitative real-time polymerase chain reaction

s.d., standard deviation

SDH, succinate dehydrogenase

SqCC, squamous cell carcinoma

TAM, tumor−associated macrophages

TCA cycle, tricarboxylic acid cycle

TGF, transforming growth factor

TME, tumor microenvironment

Treg cell, regulatory T cell

INTRODUCTION

Regulatory T (Treg) cells play a key role in maintaining peripheral immunological tolerance and controlling immune responses toward pathogens and tumors (1). In the era of tumor immunotherapy, Treg cells in tumor tissue have been widely studied because they are regarded as a potent factor in resistance to immunotherapy. The transcriptional factor forkhead box P3 (FOXP3) serves as a lineage-specific marker of Treg cells, and it plays key roles in their development, stability, and suppressive functions (2-4). In a previous paper, it was reported that loss of FOXP3 expression or mutations in *FOXP3* lead to severe lymphoproliferative autoimmune disease in both mice and humans (5, 6).

Increased Treg cell infiltration in tumor tissues is generally considered a poor prognostic marker because of their immune-suppressive functions. However, the actual prognostic value of Treg cell infiltration is inconclusive. Previous studies have identified increased Treg cell infiltration as a marker of either poor or good prognosis, while others have suggested that Treg infiltration in tumor tissues has no prognostic power (7, 8). Treg cells are functionally and phenotypically heterogeneous (9). Based on FOXP3 and CD45RA expressions, Treg cells can be dissected into three subpopulations: Fraction I ($FOXP3^{low}CD45RA^{+}$; referred to as

naive Treg cells); Fraction II (FOXP3^{high}CD45RA^{-}; referred to as effector Treg cells); Fraction III (FOXP3^{low}CD45RA^{-}; referred to as FOXP3^{+}non-Treg cells). Effector Treg (eTreg) cells are terminally differentiated, highly suppressive, and functionally stable, but FOXP3^{+}non-Treg cells do not possess suppressive activity and can secrete pro-inflammatory cytokines (9). The inconsistent clinical impacts of Treg cell infiltration in tumor tissues might partly derive from this heterogeneity of Treg cell subpopulations. Saito et al. reported that such subpopulations of Treg cells were identified in human colon cancer tissues, and that development of inflammatory FOXP3^{+}non-Treg cells might depend on the secretion of interleukin (IL)-12 and transforming growth factor (TGF)-β by tissues. These authors indirectly validated the hypothesis that a high FOXP3^{+}non-Treg cell subpopulation was related to good disease free survival (DFS), with only mRNA data of colon cancer tissue(10). A more-thorough evaluation of Treg cell infiltration is needed for predicting prognosis of tumor patients.

Each subset of immune cells utilizes different metabolic programs for their survival, activation, and differentiation (11, 12). Cytotoxic and effector T cells primarily depend on glycolysis for their proliferation and functioning. In contrast, Treg cells are less dependent on glycolysis, and instead mainly utilize oxidative phosphorylation (OXPHOS) and fatty acid

oxidation (FAO) (13, 14). Activated dendritic cells and proinflammatory tumor-associated macrophages (TAMs) predominantly use glycolysis. However, tolerogenic TAMs usually use oxygen-driven metabolic pathways, such as OXPHOS and FAO (15). Therefore, each immune cell subset might be uniquely affected under the various types of tumor metabolism.

FOXP3 modulates Treg cell metabolism to sustain its function by inducing oxidative phosphorylation and suppressing glycolysis (16). On the other hand, increased glycolysis by increasing mTORC1 activity impairs the suppressive capacity of Treg cells and decreases FOXP3 expression both in vitro and in vivo (17, 18).

The mitochondrial succinate dehydrogenase (SDH) complex is involved in both the tricarboxylic acid (TCA) cycle and electron transfer chain (mitochondrial complex II). It catalyzes the oxidation of succinate to fumarate in the TCA cycle, and feeds electrons into the respiratory chain ubiquinone (UQ) pool (19). It is known to be a key component of mitochondrial metabolism and also exhibits tumor-suppressive functions (20). SDH is composed of four different subunits: SDHA, SDHB, SDHC, and SDHD (21). Mutations or defects in each subunit result in different clinical manifestations. SDHA germline mutations can lead to Leigh syndrome, mitochondrial encephalopathy, and optic atrophy; SDHA-D

germline mutations can lead to the development of various tumors, including paraganglioma, pheochromocytoma, renal cell carcinoma, and gastrointestinal stromal tumors. In some cases of SDH germline mutations, autoimmune diseases are also reported (22). Based on the dependency of Treg cells on OXPHOS and FAO, SDH might also play a key role in Treg cells. However, it is unclear whether SDH indeed has a key role in Treg cell functionality and how SDH may regulate Treg cell biology. Among the subunits of SDH, I focused on SDHA, a starting subunit of ETC and a component of the TCA cycle.

In this study, I found that SDHA deficiency in Treg cells resulted in a scurfy phenotype in mice. SDHA-deficient Treg cells had impaired suppressive capacity and gained inflammatory functions. Their inflammatory phenotype was partly derived from increased glycolysis. SDHA-deficient Treg cells showed lower FOXP3 expression compared to that in wild-type Treg cells. This positive correlation between FOXP3 and SHDA expression was also found in human tumor tissues. Similar to SDHA-deficient Treg cells, $FOXP3^{low}$ Treg cells showed inflammatory cytokine production, and increased infiltration of this population implied better survival of patients undergoing conventional therapies or PD-1/PD-L1 immunotherapies. Therefore, our findings confirm the essential roles of SDHA in Treg cells.

MATERIALS AND METHODS

Mice

Foxp3$^{YFP-Cre}$, *Foxp3*$^{EGFP-cre-ERT2}$, and *Rag1*$^{-/-}$ mice were purchased from Jackson Laboratory. *Sdha* floxed mice (*Sdha*$^{fl/fl}$, *Sdha*$^{tm2a(KOMP)Wtsi}$) were generated at the University of California, Davis Mouse Biology Program (MBP). Strains were maintained on a C57BL/6/J background. *Foxp3*$^{YFP-Cre}$ and *Foxp3*$^{EGFP-cre-ERT2}$ mice were crossed to *Sdha*$^{fl/fl}$ mice to generate mice with SDHA-deficient Treg cells. All animals were bred and maintained in specific-pathogen-free facilities at the Biomedical Research Institute of Seoul National University Hospital. All mice experiments were conducted between 4 and 6 weeks of age, unless otherwise noted. All experiments were approved by the Institutional Animal Care and Use Committee of the Clinical Research Institute of Seoul National University Hospital (#15-0203-C2A4) and were conducted in an AAALAC International accredited facility.

Cell line and in vitro culture

The MC38 colon adenocarcinoma cell line was purchased from the Korean cell line bank. Cells were cultured in Dulbecco's Modified Eagle Medium (DMEM) supplemented with 10% fetal bovine serum (FBS) and 1% penicillin plus streptomycin and used for mouse tumor model experiments.

Patients and samples

For flow cytometry analysis, fresh tumor samples were taken from 130 lung cancer and 18 colon cancer patients. Evaluation of the relationship between immune cell infiltration and tumor cell metabolism was performed in 41 lung adenocarcinoma (ADC) patients. Evaluation of the correlation between FOXP3 and SDHA expression on regulatory cells was done in 26 lung cancer and 18 colon cancer patients. Evaluation of cytokine production from different subsets of $CD4^+$ T cells was done in 38 lung ADC and 25 lung squamous cell carcinoma (SqCC) patients. All patients underwent surgery at the Seoul National University Hospital (SNUH). All patients gave express written informed consent for sample collection and data analysis.

For immunohistochemistry (IHC) analysis, tissue microarrays were constructed from formalin-fixed paraffin-embedded (FFPE) tumor tissues from 375 lung ADC and 118 lung SqCC patients from SNUH, and 338 colon ADC patients from Asan Medical Center (AMC). For IHC analysis, informed consent for participation was waived by the institutional review boards of SNUH and AMC on the basis that this was a retrospective study using archived material and did not increase the risk to the patients. The tumor, node, metastasis (TNM) staging was performed based on the 7th American Joint Committee on Cancer (AJCC) staging system for lung cancer and the 8th AJCC system for colon cancer (23, 24). Clinicopathological features of the patients are summarized in Tables 1-3. This study followed the World Medical Association Declaration of Helsinki recommendations and was approved by the Institutional Review Board of SNUH (Nos.: H-1404-100-572 and H-1905-115-1035).

Table 1. Clinicopathological features of patients with lung ADC

Clinicopathological parameter	N (Total = 375) (%)
Median age at diagnosis (range)	64 (27−86)
Sex	
Female	189 (50.4)
Male	186 (49.6)
Smoking	
Never	234 (62.4)
Ever	141 (37.6)
T stage*	
T1	184 (49.1)
T2	161 (42.9)
T3	22 (5.9)
T4	4 (1.3)
N stage*	
N0	303 (81.5)
N1	25 (6.7)
N2	42 (11.3)
N3	2 (0.5)
M stage*	
M0	370 (98.7)
M1	5 (1.3)
AJCC 7th stage*	
I	277 (74.1)
II	43 (11.5)

III	49 (13.1)
IV	5 (1.3)
EGFR*	
WT	137 (38.4)
E19del	119 (33.3)
L858R	78 (21.8)
Other	23 (6.4)
ALK*	
Wild	351 (98.3)
Translocation	6 (1.6)
KRAS*	
Wild	331 (93.2)
Mutant	24 (6.8)

*Some cases have missing values.

Abbreviations: ALK, anaplastic lymphoma kinase; EGFR, epidermal growth factor receptor; KRAS, Kirsten rat sarcoma virus

Table 2. Clinicopathological features of patients with lung squamous cell carcinoma

Clinicopathological parameter	N (Total = 118) (%)
Median age at diagnosis (range)	67 (43–87)
Sex	
Female	7 (5.9)
Male	111 (94.1)
Smoking	
No	10 (8.5)
Yes	108 (90.5)
T stage	
T1	20 (17.0)
T2	58 (57.6)
T3	23 (19.5)
T4	7 (5.9)
N stage*	
N0	64 (55.2)
N1	32 (27.6)
N2	20 (17.2)
AJCC 7th stage*	
I	39 (33.6)
II	46 (39.7)
III	31 (26.7)

*Some cases have missing values.

Table 3. Clinicopathological features of patients with colon adenocarcinoma

Clinicopathological parameter	N (Total = 338) (%)
Median age at diagnosis (range in years)	22–85 (median, 60)
Sex	
Female	132 (39.1)
Male	206 (60.9)
Diagnosis	
Conventional CRC	334 (98.8)
HNPCC	4 (1.2)
MSI*	
MSS	294 (91.6)
MSI-L	1 (0.3)
MSI-H	26 (8.1)
Differentiation*	
WD	47 (13.9)
MD	271 (80.4)
PD	19 (5.6)
T stage	
T1	27 (8.0)
T2	42 (12.4)
T3	254 (75.1)
T4	15 (4.4)
N stage	
N0	204 (60.4)

N1	95 (28.1)
N2	39 (11.5)
M stage	
M0	297 (87.9)
M1	41 (12.1)
AJCC 8th	
I	60 (17.8)
II	138 (40.8)
III	99 (29.3)
IV	41 (12.1)
LVI	
Not identified	246 (72.8)
Present	92 (17.2)
Neural invasion	
Not identified	257 (76.0)
Present	81 (24.0)

Abbreviations: CRC, colorectal cancer; HNPCC, hereditary nonpolyposis colorectal cancer; MSI, microsatellite instability; MSS, Microsatellite stable; WD, well differentiated; MD, moderately differentiated; PD, poorly differentiated; LVI, lymphovascular invasion

Histology

Tissues and organs from age-matched wild-type and experimental mice were fixed in 10% formalin and paraffin-embedded. Sections of paraffin-embedded tissue were stained with hematoxylin and eosin (HE). Two independent pathologists who were blinded to the experimental conditions performed the microscopic evaluations.

Immunohistochemistry (IHC)

IHC was performed using rabbit anti-CD8 monoclonal (clone SP16, Thermo Fisher Scientific) and rabbit anti-FOXP3 monoclonal (236A/E7, Abcam) antibodies. Immunostaining was performed using the Benchmark XT autostainer (Ventana Medical Systems, Tucson, AZ, USA). The numbers of $CD8^+$ and $FOXP3^+$ tumor-infiltrating lymphocytes (TILs) per mm^2 were automatically enumerated by modified nuclear algorithms in Aperio ImageScope software (Aperio Technologies, Vista, CA, USA).

Flow cytometry, cell sorting, and immune subset analysis

To analyze tumor-infiltrating immune cell subsets, about 1 gram of fresh human lung cancer tissue was minced using sterile blades, digested in RPMI-1640 supplemented with 80 U/mL DNase I, 300 U/mL collagenase I, and 60 U/mL hyaluronidase at 37 ℃ for 30 min, and then filtered using a 70-μm cell strainer. After red blood cell (RBC) lysis,

cells were stained for dead cell exclusion using an amine-reactive fluorescent dye (Zombie Aqua™ Fixable Viability Kit) and then pre-incubated with an Fc receptor blocking solution to reduce non-specific binding. Cells were stained using the appropriate antibodies in flow cytometry staining buffer for at least 30 min at 4 °C, in the dark. To analyze immune cell populations of mouse lymphoid tissues, thymus, spleen, and lymph nodes were crushed into single-cell suspensions with a 40-μm cell strainer. After RBC lysis and Fc receptor blocking, cells were stained with appropriate FACS antibodies. For intracellular cytokine staining, 1-2 x 10^6 cells were stimulated in RPMI medium containing 200 ng/mL Phorbol myristate acetate (PMA), 1 μg/mL ionomycin, and 1 μL GolgiStop for 4 hours. The antibodies used in the experiments are listed in Table 4. Data were analyzed using FlowJo v10.1 (Treestar), and the gating strategy is shown in Figure 1.

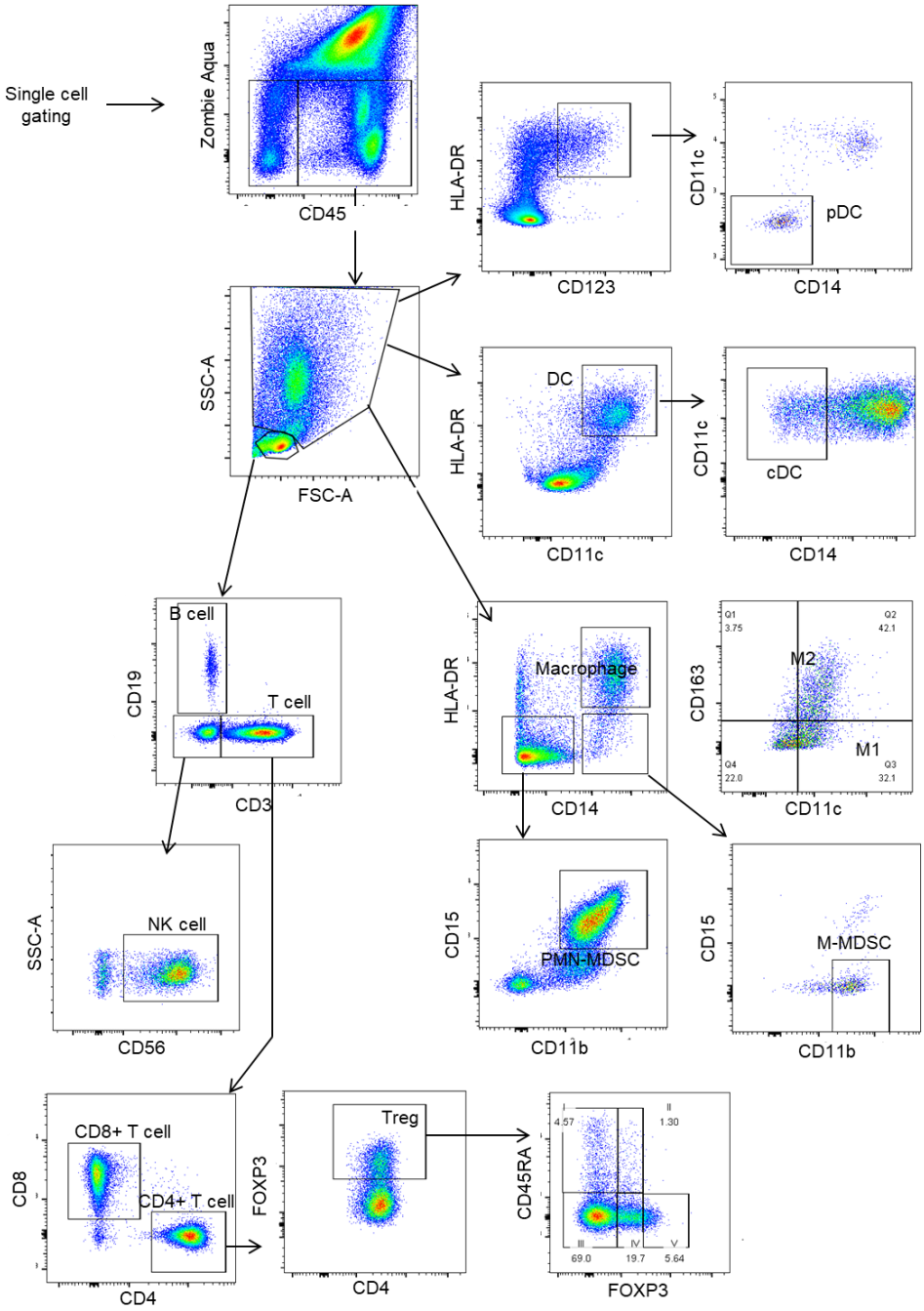

Figure 1. Gating strategy for human cancer tissues.

Enzyme-linked immunosorbent assay

Cytokine levels in culture supernatants were evaluated using the OptEIA enzyme-linked immunosorbent assay (ELISA) Kit (BD Biosciences) according to the manufacturer's protocol. Interferon (IFN)-γ, IL-4, and IL-17A from Treg cells were measured. The reagents and antibodies used in this experiment are listed in Table 4.

Treg cell-mediated suppression assays

The CellTrace™ Violet (CTV) cell proliferation kit (Thermo Fisher Scientific) was used to assess Treg cell suppression capacity. Freshly sorted YFP^{+} Treg cells from *Foxp3*$^{YFP-Cre}$ mice and *Foxp3*$^{YFP-Cre}$*Sdha*$^{fl/fl}$ mice obtained by flow cytometry were co-cultured with CTV-stained Foxp3-YFP^{-} T cells at various ratios in U-bottomed 96-well plates in the presence of plate-coated 0.5 μg/mL anti-CD3 and 2.5 μg/mL soluble anti-CD28 mAb. The proliferation of CTV-stained $YFP^{-}CD4^{+}$ Tconv cells was assessed 3 days later using flow cytometry.

Quantitative real-time PCR (qRT-PCR)

Total RNA was isolated using TRIzol reagent (Invitrogen) according to the manufacturer's protocol. RNA was reverse transcribed into cDNA constructs using Maloney murine leukemia virus reverse transcriptase

Taq polymerase (Promega). For qRT-PCR, PCR products were quantified using an Applied Biosystems 7500 Sequence Detection System (Applied Biosystems). Expression levels were normalized to that of 18S rRNA. Primers used for real-time PCR are listed in Table 5.

Metabolomic analysis

Metabolites were extracted according to previously described methods (25, 26), followed by MeOX and MTBSTFA derivatization. Briefly, metabolites were extracted using cold (−80 °C) methanol:water (80:20 v/v). The remaining supernatant was removed and cells were gently rinsed twice with 2 mL of ice-cold isotonic saline solution (9 g/L NaCl), and thereafter maintained on ice throughout the procedure. After the saline washes, cells were transferred onto dry ice and 1000 μL of −80 °C methanol was added. Cell suspensions were quickly vortexed and then sonicated in an ice bath for 10 min (30s ON, 30s OFF) on the "high" setting using the BioRuptor (UCD-200 TM, Diagenode). GC-MS/MS dynamic multiple-reaction monitoring (dMRM) analyses were performed using the Agilent 7890/7000 GC triple quadrupole mass spectrometer system. Gas chromatography was carried out using an Agilent J&W HP-5ms UI 15 m × 0.25 mm × 0.25 μm (P/N 19091S-431UI) capillary column. Helium was used as the carrier gas, with a constant column flow rate of

1.5 mL/min. The initial oven temperature of 60 °C was increased to 320 °C at a rate of 10 °C/min. The mass spectrometer was operated in electron-ionization mode at 70 eV, and analyses were performed in dMRM mode. The area ratios between the analyte and the internal standard were used for the evaluations. The split/splitless injector temperature was set to 280 °C. The samples were injected in splitless mode with an auto-sampler Agilent 7683A injector. Agilent MassHunter data-acquisition software (Ver. B.04.00) was used for the data acquisition, and MassHunter Workstation software for quantitative analysis (QQQ) was used for quantitative analysis. Data from metabolic profiling by GC-MS/MS were normalized by total protein concentration.

Rag1 KO mice Treg cell adoptive transfer

For adoptive transfer of Treg cells, $5x10^5$ FACS-sorted wild-type or *Sdha* knockout (KO) Treg cells were injected intravenously into each $Rag1^{-/-}$ mouse. $Rag1^{-/-}$ mice were sacrificed at 8 weeks after transfer.

Mouse tumor model

For tumor experiments, $5x10^5$ cells of MC38 colon cancer cells were subcutaneously injected into the flank of 8- to 12-week-old wild-type ($Foxp3^{EGFP-cre-ERT2}$) and *Sdha* inducible knockout (*Sdha* iKO,

Sdha$^{fl/fl}$*Foxp3*$^{EGFP-cre-ERT2}$) mice, and the mice were sacrificed on day 17 for flow cytometric analysis. To establish *Sdha* iKO mice, 100 μL of 20 mg/mL tamoxifen dissolved in corn oil with 5% Ethanol was administered intraperitoneally on days 3, 4, 6, 7, and 8 after tumor inoculation. Harvested tumor tissues were subjected to flow cytometric analysis.

Statistical analysis

P values were calculated as described in individual figure legends using Graphpad Prism 7 (Graphpad Software) or SPSS Statistics 26 (IBM). *P* values < 0.05 were considered statistically significant. Data are presented as mean ± s.d., unless specifically stated otherwise in the figure legend. The numbers of biological and/or technical replicates are also expressly stated in the figure legends. Littermates were used in experiments whenever possible. All images are representative of at least two independent experiments on mice of the same genotype.

Table 4. Key materials and antibodies

Antibodies for flow cytometry	Source
Zombie Aqua™ Fixable Viability Kit	Biolegend
Hu BD Fc Block Pure Fc1	BD Pharmingen™
PerCP anti-mouse CD45	Biolegend
PE/Cyanine7 anti-mouse TCRβ chain	Biolegend
APC anti-mouse CD4	Biolegend
APC anti-mouse IFN-γ	Biolegend
PE anti-mouse IL-4	Biolegend
Brilliant Violet 421™ anti-mouse IL-17A	Biolegend
FITC anti-mouse IL-10	Biolegend
PE/Cyanine7 anti-mouse T-bet	Biolegend
PE anti-mouse GATA3	Biolegend
APC anti-mouse ROR-γ	Invitrogen
PE anti-mouse CD279 (PD-1)	Biolegend
APC anti-mouse CD152(CTLA-4)	Biolegend
Alexa Fluor® 700 anti-mouse/human CD11b	Biolegend
APC anti-mouse F4/80	Biolegend
Brilliant Violet 421™ anti-mouse MHCII	Biolegend
FITC anti-mouse CD206	Biolegend
PE/Cyanine7 anti-mouse CD11c	Biolegend
PE anti-mouse CD170 (Siglec-F)	Biolegend
PerCP/Cyanine5.5 anti-mouse Ly-6G	Biolegend
Brilliant Violet 421™ anti-mouse Ly-6C	Biolegend

PerCP-Cyanine5.5 anti-mouse FOXP3	Invitrogen
anti-CD45-Alexa 700	Biolegend
PerCP anti-human CD3	Biolegend
FITC anti-human CD4	Biolegend
APC/Cyanine7 anti-human CD8	Biolegend
BV421 anti-human CD19	Biolegend
APC anti-human CD56	Biolegend
Brilliant Violet 711™ anti-human CD45RA	Biolegend
PE anti-human FOXP3	Biolegend
BV786 anti-human HLA-DR	Biolegend
PE/Cyanine7 anti-human CD11c	Biolegend
FITC anti-human CD14	Biolegend
APC/Cyanine7 anti-human CD1c	Biolegend
PE anti-human CD141	Biolegend
BV650 anti-human CD123	Biolegend
APC anti-human CD15	Biolegend
BV421 anti-human IFN-γ	Biolegend
PE/Cyanine7 anti-human IL-17A	Biolegend
APC anti-human IL-4	Biolegend
Alexa Fluor® 488 Anti-SDHA	Abcam
MitoSOX™ Red Mitochondrial Superoxide Indicator	Invitrogen
MitoTracker™ Red FM	Invitrogen
Cell Trace Violet (CTV) cell proliferation kit	Thermo Fisher Scientific
Antibodies for IHC	

CD8 Monoclonal Antibody	Invitrogen
Recombinant Anti-FOXP3 antibody	Abcam
Others	
BD Pharmingen™ Purified Hamster Anti-Mouse CD3e	BD Pharmingen™
Purified NA/LE Hamster Anti-Mouse CD28	BD Pharmingen™
Reagents and Antibodies for ELISA	
OptEIA enzyme-linked immunosorbent assay (ELISA) Kit	BD Pharmingen™
BD Pharmingen™ Purified Rat Anti-Mouse IFN-γ	BD Pharmingen™
Biotin Anti-Mouse IFN-γ	BD Pharmingen™
BD Pharmingen™ Purified Rat Anti-Mouse IL-4	BD Pharmingen™
BD Pharmingen™ Biotin Rat Anti-Mouse IL-4	BD Pharmingen™
Mouse IL-17A DuoSet ELISA kit	Biotechne
Streptavidin HRP	BD Pharmingen™
Chemicals, peptides, and recombinant proteins	
RBC Lysis Buffer 10X	Biolegend
Phorbol 12-myristate 13-acetate (PMA)	Sigma
Ionomycin	Sigma
GolgiStop™	BD Pharmingen™
RPMI 1640	Biowest
DMEM	Biowest
FBS	Biowest
Penicillin/streptomycin	Biowest

D-(+)-Glucose	Sigma
2-Deoxy-D-glucose	Sigma

Table 5. Primers for qRT-PCR

Gene		Sequences
Slc2a1	F	5'-GAGACCAAAGCGTGGTGAGT-3'
(GLUT1)	R	5'-GCAGTTCGGCTATAACACT GG-3'
Slc2a3	F	5'-ATCGTGGCATAGATCGGTTC-3'
(GLUT3)	R	5'-TCTCAGCAGCTCTCTGGGAT-3'
Hk2	F	5'-TGATCGCCTGCTTATTCACGG-3'
	R	5'-AACCGCCTAGAAATCTCCAGA-3'
Pfkm	F	5'-TGTGGTCCGAGTTGGTATCTT-3'
	R	5'-GCACTTCCAATCACTGTGCC-3'
Ldha	F	5'-TATCTTAATGAAGGACTTGGCGGATGAG-3'
	R	5'-GGAGTTCGCAGTTACACAGTAGTC-3'
Gapdh	F	5'-TTGATGGCAACAATCTCCAC-3'
	R	5'-CGTCCCGTAGACAAAATGGT-3'
18S rNRA	F	5'-CGGCGACGACCCATTCGAAC-3'
	R	5'-GAATCGAACCCTGATTCCCCGT-3'

Abbreviations: F, forward; R, reverse

RESULTS

Tumor glycolysis is differentially associated with each subset of immune cells.

Using flow cytometry, tumor-infiltrating lymphoid cells and myeloid cells from fresh lung ADC tissues from 41 patients were comprehensively profiled (Figure 1). IHC was used to evaluate hexokinase 2 (HK2) expression in tumor cells as an indicator of tumor glycolysis, because HK2 is both the first and the rate-limiting enzyme in glycolysis. The experimental scheme is described in Figure 2A, and the correlations between individual immune cell subsets and tumor HK2 expression are summarized in Fig. 2B-C and Table 6. Total immune cell infiltration did not differ when quantified according to tumor HK2 expression. The proportion of $CD3^+$ cells to total immune cells and $CD4^+$ T cells to total immune cells tended to be inversely correlated with HK2 tumor expression (spearman rho = −0.283, $P = 0.077$ and spearman rho = −0.326, $P = 0.040$, respectively). The proportion of $CD19^+$ B cells to total immune cells was also inversely correlated with HK2 tumor expression (spearman rho = −0.377, $P = 0.017$; Table 6). Although the proportion of Treg cells to total immune cells did not significantly differ according to tumor HK2 expression, the proportion of Treg cells to $CD4^+$ T cells showed a

significant positive correlation with tumor HK2 expression (spearman rho = 0.480, P = 0.003). Of note, the ratio of $CD8^+$ T cells to Treg cells was inversely correlated with tumor HK2 expression (spearman rho = −0.415, P = 0.012) (Fig. 2B). Proportions of tumor−infiltrating macrophages, dendritic cells, and myeloid−derived suppressor cells (MDSCs) did not differ according to tumor HK2 expression (Fig. 2C). In addition, tumor HK2 expression did not affect M1 versus M2 polarization of macrophages (Table 5). Collectively, tumor HK2 expression, which is indicative of tumoral glycolysis, was more closely related to lymphoid cell infiltration than to myeloid cell infiltration. Therefore, we further validated the association between tumor HK2 expression and CD8+ T cells, Treg cells, and their ratios in additional larger cohorts.

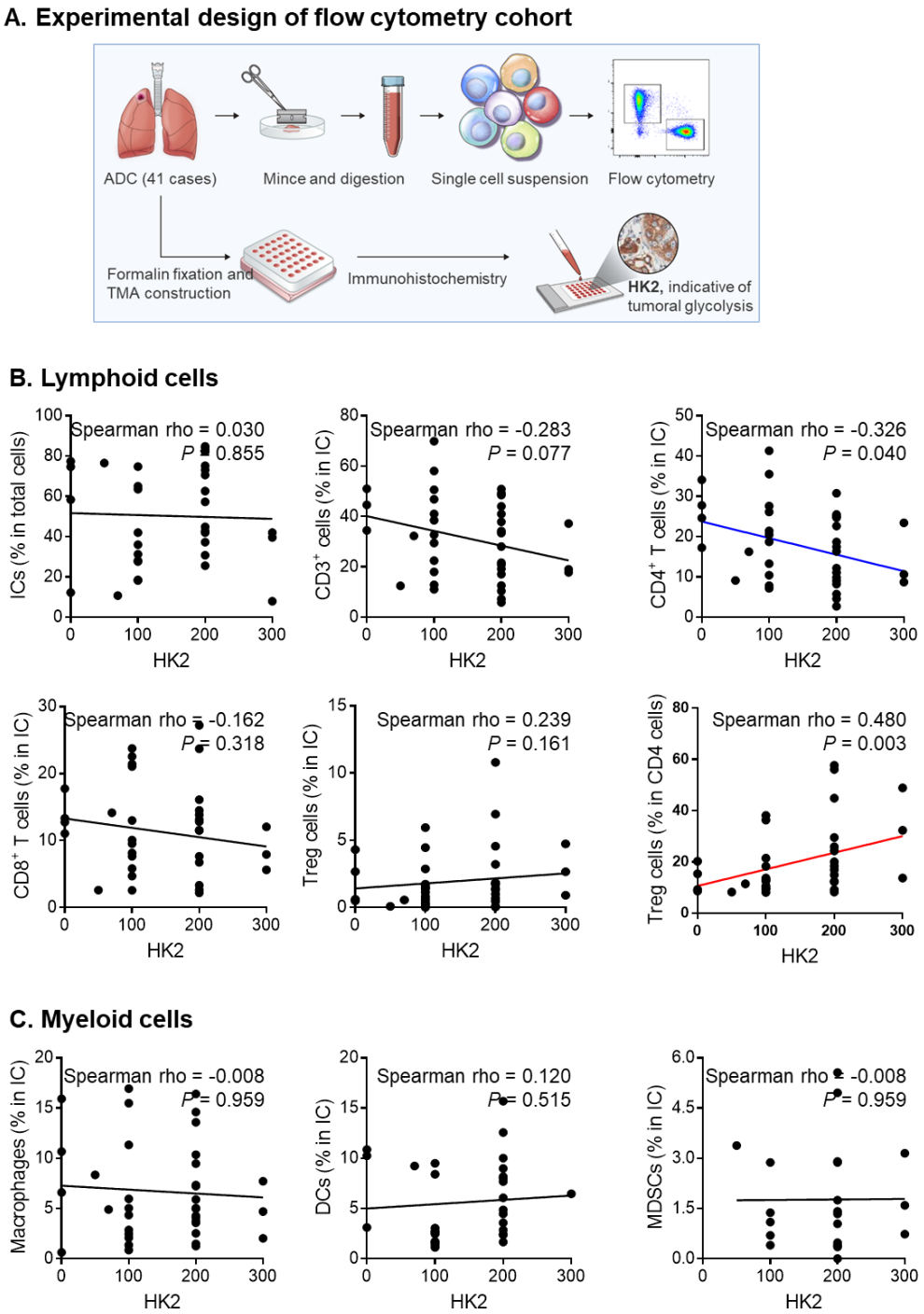

Figure 2. The relationship between tumor HK2 expression and tumor-

infiltrating immune cell subsets as analyzed by flow cytometry. A. Experimental design for flow cytometry. **B.** Total immune cell and lymphoid cell infiltration statuses according to tumor HK2 expression. **C.** Myeloid cell infiltration according to tumor HK2 expression. All *P* values were calculated using Spearman correlation analysis.

Table 6. Correlations between tumor HK2 expression and immune cell subsets

Immune cell subset	Correlation coefficient*	*P* value
Pan−immune cells (% of total cells)	0.030	0.855
$CD3^+$ cells (% of ICs)	−0.283	0.077
$CD4^+$ T cells (% of CD3+ cells)	−0.225	0.162
$CD4^+$ T cells (% of ICs)	−0.326	0.040
$CD8^+$ T cells (% of $CD3^+$ cells)	0.114	0.485
$CD8^+$ cells (% of ICs)	−0.162	0.318
Treg cells(% of $CD4^+$ cells)	0.480	0.003
Treg cells (% of ICs)	0.239	0.161
$CD8^+$ T cells to Treg cells ratio	−0.415	0.012
$CD19^+$ cells (% of ICs)	−0.377	0.017
NK cells (% of ICs)	−0.134	0.411
Macrophages (% of ICs)	0.023	0.888
M0 (% of macrophages)	−0.116	0.477
M1 (% of macrophages)	0.089	0.584
M2 (% of macrophages)	−0.010	0.949
DCs (% of ICs)	0.091	0.604
MDSCs	0.028	0.901

*Spearman correlation analysis

Abbreviations: ICs, immune cells; Tregs, regulatory T cells; DCs, dendritic cells; MDSCs, myeloid−derived suppressor cells; NK cells, Natural killer cells

Infiltration of Treg cells was positively correlated with tumor HK2 expression.

To validate the above findings, I evaluated the correlations between HK2 expression in tumor cells and the numbers of $CD8^+$ cells and Treg cells ($FOXP3^+$ cells) in tumors using IHC in 375 lung ADC, 118 lung SqCC, and 338 colon ADC cases, as schematically described in Fig. 3A. HK2 expression was correlated with some clinicopathological parameters with marginal statistical significance. The relationships of tumor HK2 expression with $CD8^+$ cells, Treg cells, and their ratio are summarized in Fig. 3B–D. $CD8^+$ cell infiltration was not consistently correlated with tumor HK2 expression in three tumor cohorts. In contrast, Treg cell infiltration was positively correlated with tumor HK2 expression in the lung ADC and SqCC cohorts (lung ADC spearman rho = 0.489, $P < 0.001$; lung SqCC spearman rho = 0.306, $P = 0.001$), and tended to be positively correlated with tumor HK2 expression in the colon ADC cohort (spearman rho = 0.111, $P = 0.054$) (Fig. 3B–D). Of note, the ratios of $CD8^+$ T cells to Treg cells were inversely correlated with HK2 tumor expression (lung ADC spearman rho = −0.335, $P < 0.001$; lung SqCC spearman rho = −0.236, $P = 0.010$; colon ADC spearman rho = −0.175, $P = 0.004$) (Fig. 3B–D). Representative IHC images are presented in Figure 3E. These findings were consistent with those of the flow cytometry analyses and

demonstrated that an increase in tumor glycolysis, as represented by tumor HK2 expression, was inversely correlated with the ratio of $CD8^+$ T cells to Treg cells in patients with lung cancer and colon cancer. These findings suggest that Treg cells might outcompete $CD8^+$ T cells in low-available-glucose and acidic environments.

A. Experimental design of validation cohorts

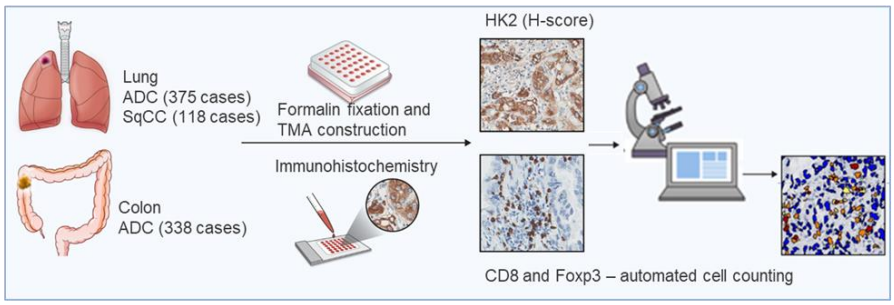

B. Lung ADC

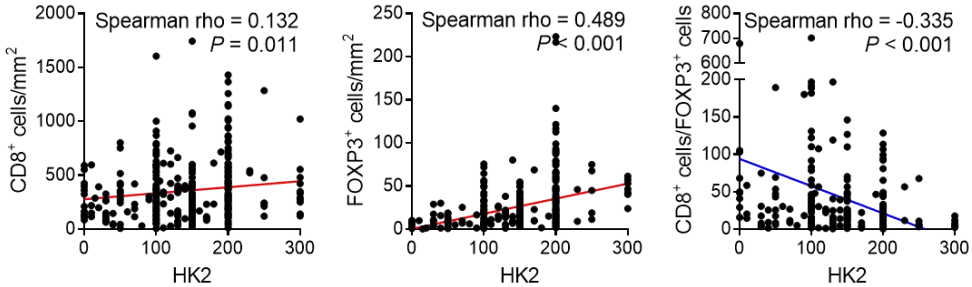

C. Lung SqCC

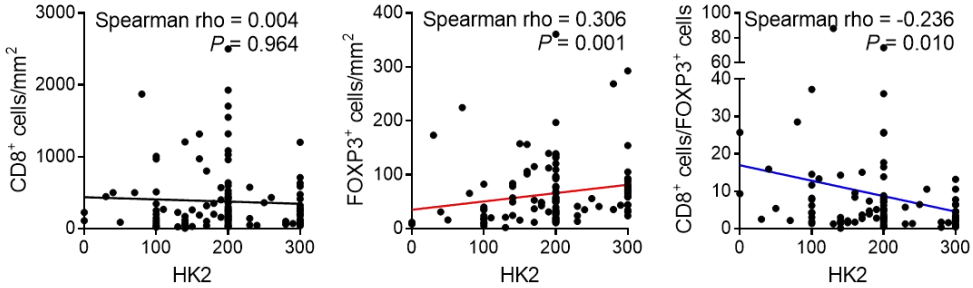

D. Colon ADC

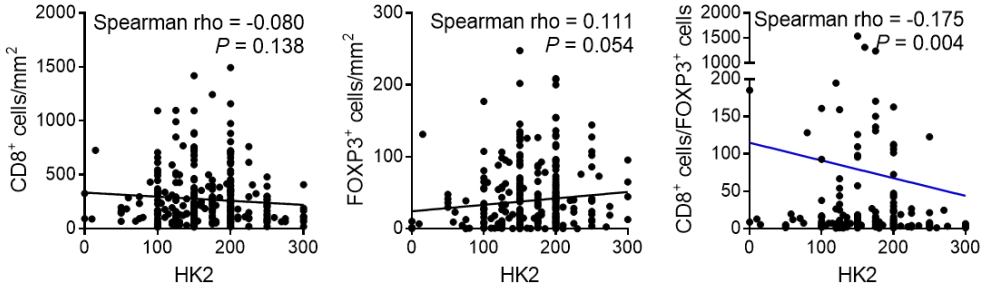

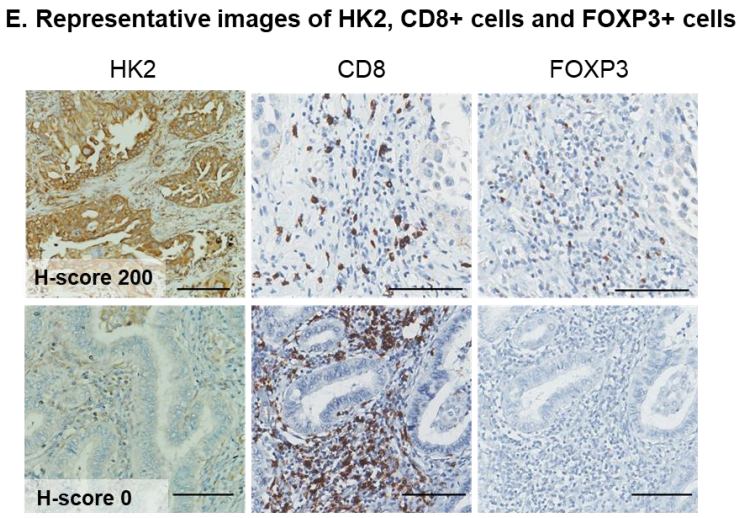

Figure 3. Correlation between HK2 tumor expression and immune cell composition including CD8$^+$ cells, Treg cells, and ratio of CD8$^+$ cells to Treg cells. A. Experimental design of the validation cohorts. Results from **B.** 375 lung ADC patients, **C.** 118 lung SqCC patients, and **D.** 338 colon ADC patients. **E.** Representative images of tumor HK2 expression relative to CD8$^+$ T cells and Treg cells; high tumor HK2 expression with a low ratio of CD8$^+$ cells to Treg cells (upper) and low tumor HK2 expression with a high ratio of CD8$^+$ cells to Treg cells. (Original magnification: 200×, bar = 100 μm). All *P* values were calculated using Spearman correlation analysis.

Sdha$^{fl/fl}$*Foxp3*$^{YFP-Cre}$ mice showed a scurfy-like phenotype.

Based on the above findings as well as those of previous studies (11, 14, 27), Treg cells are relatively insusceptible to low-available-glucose and acidic environments, and instead depend more on mitochondrial metabolism, including OXPHOS and fatty acid oxidation. SDH is a key component of mitochondrial metabolism and is involved in both the TCA cycle and the ETC. Therefore, identifying the influences of SDH on Treg cells is important for understanding the biology of Treg cells in the era of tumor immunology.

To identify the role of SDHA in Treg cells, I generated *Sdha*$^{fl/fl}$*Foxp3*$^{YFP-Cre}$ mice. Before the age of 4 weeks, nearly all mice exhibited a scurfy phenotype. They showed severe skin inflammation and were underweight (Figure 4A-B). All mice died before the age of 8 weeks because of severe inflammation throughout the body (Figure 4C). Upon dissection, the thymus was found to be atrophied, and the spleen and lymph nodes were significantly enlarged in *Sdha*$^{fl/fl}$*Foxp3*$^{YFP-Cre}$ mice as compared to wild-type (*Foxp3*$^{YFP-Cre}$) mice. The total cell counts of the thymus, spleen, and lymph nodes reflected the sizes of the organs (Figure 4D-E). Marked inflammatory cell infiltration was observed in various organs (Figure 4F). *Sdha*$^{fl/fl}$*Foxp3*$^{YFP-Cre}$ mice had more INF-γ-, IL-17A- and IL-4-secreting CD4^{+} T cells than the wild-type mice

(Figure 4G). Moreover, more effector $CD4^+$ T cells ($CD44^{high}CD62L^{low}$) and less naïve $CD4^+$ T cells ($CD44^{low}CD62L^{high}$) were observed in the spleen and lymph nodes of *Sdha*$^{fl/fl}$*Foxp3*$^{YFP-Cre}$ mice as compared to wild-type mice (Figure 4H). These findings suggest that SDHA might play a role in maintaining suppressive capacity of Treg cells and peripheral homeostasis.

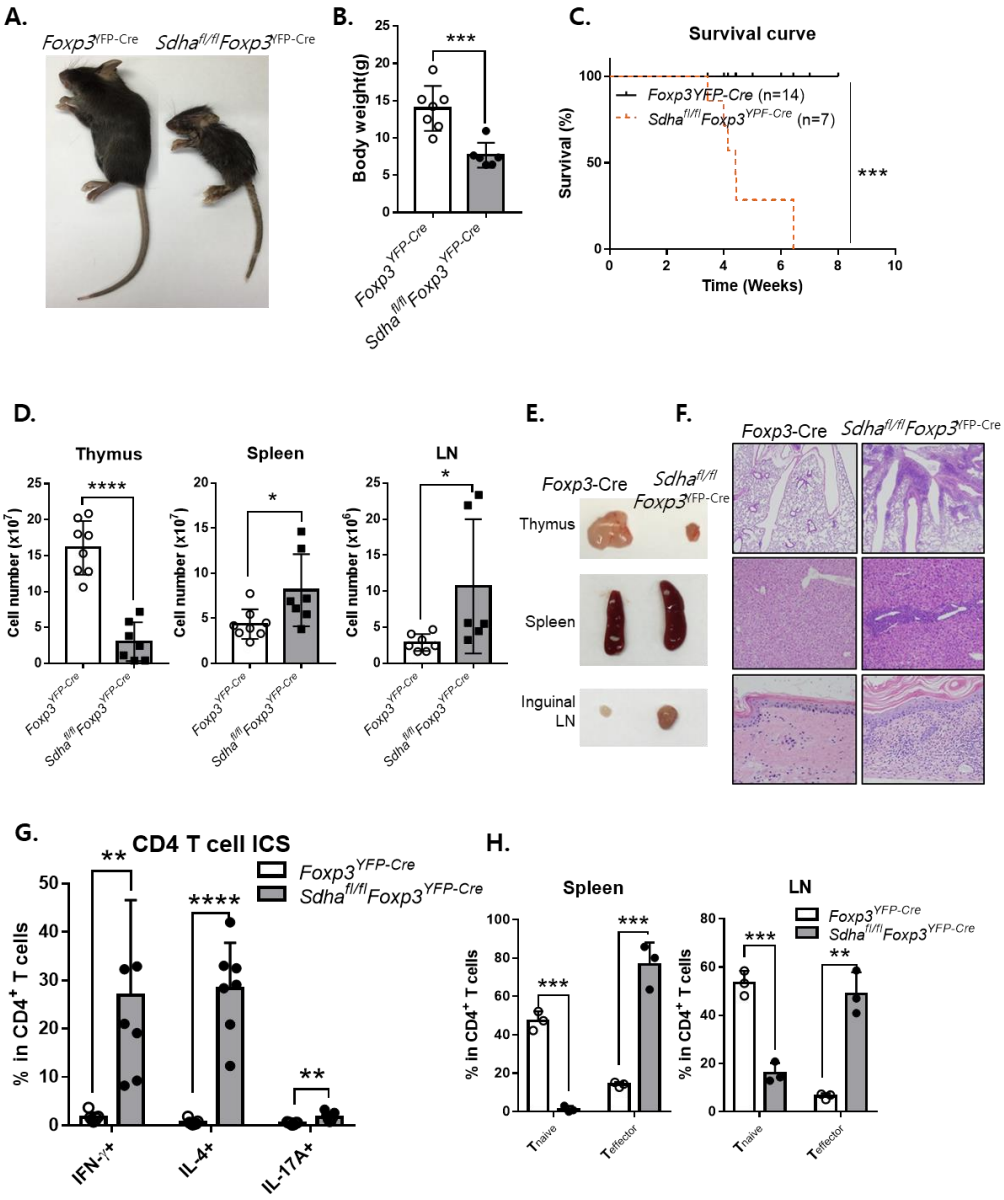

Figure 4. *Sdha*$^{fl/fl}$*Foxp3*$^{YFP-Cre}$ mice showed a scurfy-like phenotype. A. Representative images of a wild-type mouse (*Foxp3*$^{YFP-Cre}$) and a *Sdha*$^{fl/fl}$*Foxp3*$^{YFP-Cre}$ mouse at 3 weeks of age. *Sdha*$^{fl/fl}$*Foxp3*$^{YFP-Cre}$ mice

were smaller than the wild-type mice and had severe skin ulceration all over their bodies **B.** *Sdha*$^{fl/fl}$*Foxp3*$^{YFP-Cre}$ mice (n = 7) had lower body masses than the wild-type mice (n = 7). **C.** Survival of wild-type mice (n = 14) and *Sdha*$^{fl/fl}$*Foxp3*$^{YFP-Cre}$ mice (n = 7) **D.** Numbers of total cells in the thymus, spleen, and lymph nodes of the four-week-old wild-type (n = 8) and *Sdha*$^{fl/fl}$*Foxp3*$^{YFP-Cre}$ mice (n = 6). **E.** Representative images of the thymus, spleen, and lymph nodes. **F.** Representative images of HE-stained lung, liver, and skin tissues from wild-type and *Sdha*$^{fl/fl}$*Foxp3*$^{YFP-Cre}$ mice at 4 weeks of age. **G.** Proportions of effector and naive $CD4^+$ T cells in wild-type (n = 3) and *Sdha*$^{fl/fl}$*Foxp3*$^{YFP-Cre}$ (n = 3) mice. **H.** Cytokine secretion of $CD4^+$ T cells in wild-type (n = 7) and *Sdha*$^{fl/fl}$*Foxp3*$^{YFP-Cre}$ (n = 7) mice. Data in parts B, D, E, and F are given as mean ± s.d., and were analyzed with two-tailed t-tests. Each cell type was analyzed individually, without assuming a constant s.d. (*$P < 0.05$, **$P < 0.01$, ***$P < 0.001$). All data points on the graphs represent individual mice isolated and analyzed on at least two different days.

SDHA-deficiency in Treg cells reduced Treg cell development and downregulated FOXP3 expression.

To evaluate the role of SDHA in Treg cell development, I counted and compared Treg cell populations in wild-type and *Sdha*$^{fl/fl}$*Foxp3*$^{YFP-Cre}$ mice. Even though the absolute counts of Treg cells were similar between the two groups, the ratio of Treg/CD4^{+} T cells was lower in the *Sdha*$^{fl/fl}$*Foxp3*$^{YFP-Cre}$ mice than in the wild-type mice (Figure 5A-B). Moreover, natural Treg (NRP1^{+}YFP^{+}CD4^{+}, nTreg) cells, which develop from the thymus, were lower in peripheral lymphoid organs in *Sdha*$^{fl/fl}$*Foxp3*$^{YFP-Cre}$ mice compared to wild-type mice, but were not completely obliterated in the *Sdha*$^{fl/fl}$*Foxp3*$^{YFP-Cre}$ mice (Figure 5C). In contrast, the number of induced Treg (NRP1^{-}YFP^{+}CD4^{+}, iTreg) cells in the lymph nodes was higher in the *Sdha*$^{fl/fl}$*Foxp3*$^{YFP-Cre}$ mice than in the wild-type mice (Figure 5C). These results imply that SDHA has a role in the development of Treg cells, but that it is not necessarily the only factor. A more detailed study evaluating thymic development of Treg cells is needed. In addition, Treg cells from *Sdha*$^{fl/fl}$*Foxp3*$^{YFP-Cre}$ mice had lower expression of FOXP3, a master transcription factor of Treg cells, as compared to that in wild-type mice (Figure 5D).

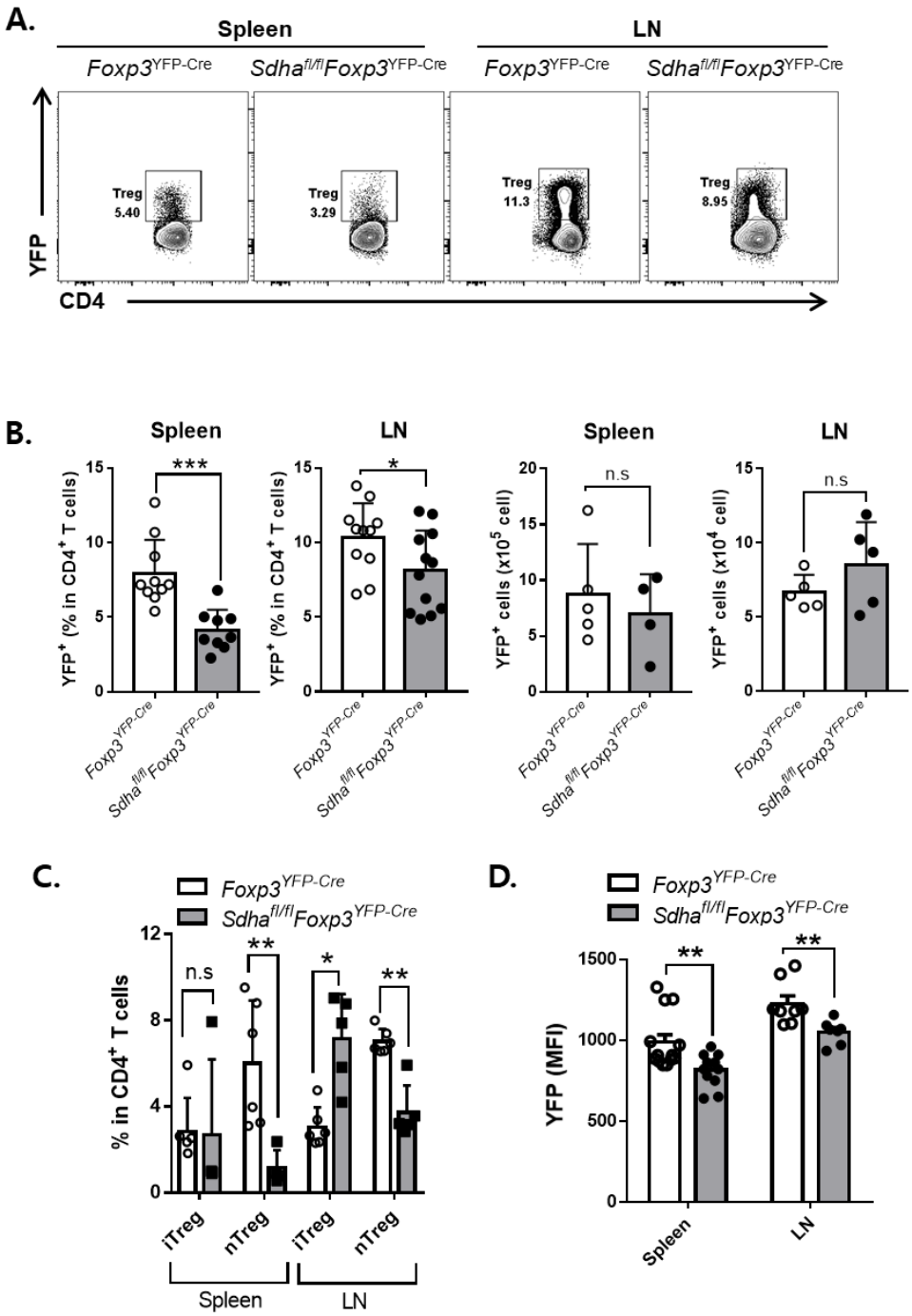

Figure 5. SDHA-deficiency in Treg cells reduced Treg cell development and downregulated FOXP3 expression. A-B. Numbers of Treg cells in

the spleen and lymph nodes in wild-type (n = 10) and *Sdha*$^{fl/fl}$*Foxp3*$^{YFP-Cre}$ mice (n = 9). **C.** Ratios of induced Treg cells (NRP1^{-}YFP^{+}CD4^{+}, iTreg) to natural Treg cells (NRP1^{+}YFP^{+}CD4^{+}, nTreg) in wild-type (n = 6) and *Sdha*$^{fl/fl}$*Foxp3*$^{YFP-Cre}$ mice (n = 5). **D.** FOXP3 (YFP) expression of Treg cells in wild-type (n = 11) and *Sdha*$^{fl/fl}$*Foxp3*$^{YFP-Cre}$ (n = 11) mice. Data in B-D are given as mean ± s.d. and were analyzed with two-tailed t-tests without assuming a constant s.d. (*P < 0.05, **P < 0.01, ***P < 0.001). All data points on the graphs represent individual mice isolated and analyzed on at least two different days.

Suppressive activity of Treg cells was decreased in *Sdha*$^{fl/fl}$*Foxp3*$^{YFP-Cre}$ mice.

To explore the role of SDHA in the suppressive function of Treg cells, I studied the suppressive capacity of Treg cells by assessing the proliferation of naïve FOXP3^{-}CD4^{+} cells co-cultured with Treg cells. Treg cells from *Sdha*$^{fl/fl}$*Foxp3*$^{YFP-Cre}$ mice showed significantly lower capacity for suppressing naïve FOXP3^{-}CD4^{+} cell proliferation in vitro as compared to Treg cells from wild-type mice (Figure 6A-B). Moreover, I compared the expression of Treg-specific effector molecules. The levels of PD-1 and CTLA-4 expression were lower in Treg cells from *Sdha*$^{fl/fl}$*Foxp3*$^{YFP-Cre}$ mice than in Treg cells from wild-type mice. These findings suggest that SDHA plays a role in maintaining the suppressive capacity of Treg cells.

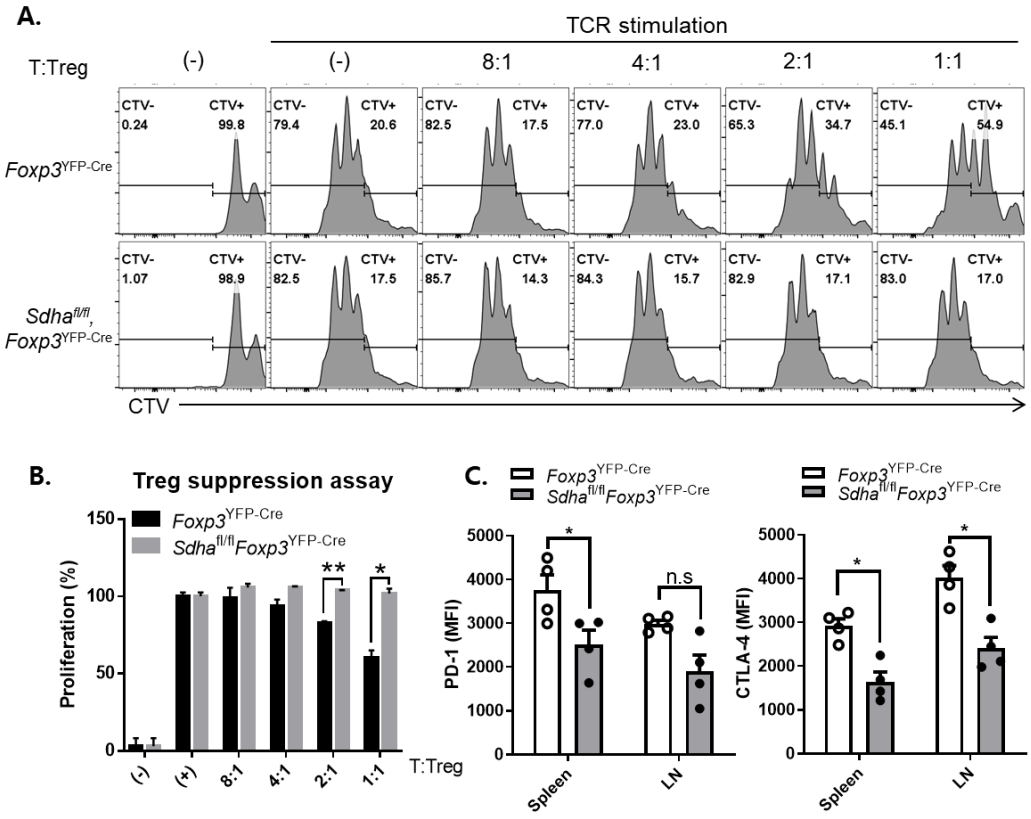

Figure 6. Suppressive activity of Treg cells was decreased in *Sdha*$^{fl/fl}$*Foxp3*$^{YFP-Cre}$ mice. A–B. The suppressive activity of Treg cells was assessed via measurement of the proliferation of naive CD4^{+} T cells in the presence of plate-coated 0.5 μg/mL anti-CD3 and 2.5 μg/mL soluble anti-CD28 mAb. Proliferation was measured as the dilution of CellTrace™ Violet (CTV) at day 3. **C.** Suppressive surface molecules of Treg cells in wild-type (n = 4) and *Sdha*$^{fl/fl}$*Foxp3*$^{YFP-Cre}$ (n = 4) mice. Data were analyzed with two-tailed t-tests. Each cell type was analyzed individually, without assuming a constant s.d. (*$P < 0.05$).

SDHA deficiency in Treg cells induces inflammatory cytokine production and helper T cell (Th)−like transcription factor expression.

After observing the decreased suppressive capacity, I further examined the production of inflammatory cytokines by Treg cells. I found that a remarkable portion of Treg cells from *Sdha*$^{fl/fl}$*Foxp3*$^{YFP-Cre}$ mice produced inflammatory cytokines, especially IFN−γ and IL−4 (Fig. 7A−B). Moreover, the total amounts of IFN−γ and IL−4 secreted from Treg cells was significantly higher in *Sdha*$^{fl/fl}$*Foxp3*$^{YFP-Cre}$ mice than in wild−type mice (Figure 7C). The total amounts of IL−17A secreted showed a similar tendency, but the difference was not statistically significant. Treg cells of *Sdha*$^{fl/fl}$*Foxp3*$^{YFP-Cre}$ mice demonstrated increased expression of Th1 and Th2 transcription factors (TBX21 and GATA3) but not of Th17 transcription factor (RORγ), as compared to their expression levels in wild−type mice (Figure 7 D−E).

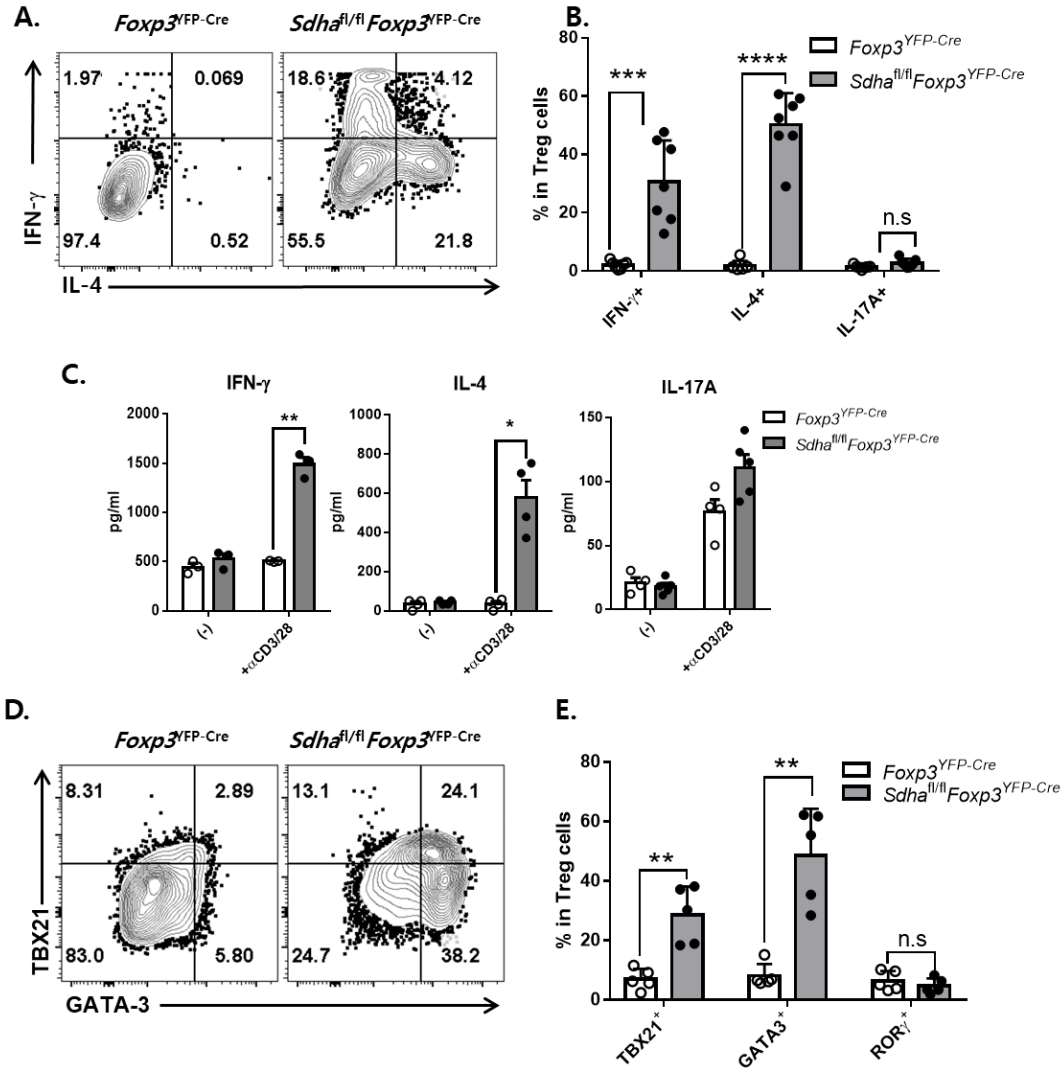

Figure 7. SDHA deficiency in Treg cells induces inflammatory cytokine production and helper T cell (Th)-like transcription factor expression. A-B. Proportions of cytokine-producing Treg cells in wild-type (n = 7) and *Sdha*$^{fl/fl}$*Foxp3*$^{YFP-Cre}$ (n = 7) mice. C. Total amounts of IFN-γ, IL-4, and IL-17A in purified Treg cells from wild-type (n = 4) and

Sdha$^{fl/fl}$*Foxp3*$^{YFP-Cre}$ (n = 5) mice. **D–E.** TBX21, GATA3, and RORγ expressions in Treg cells of wild-type (n = 5) and *Sdha*$^{fl/fl}$*Foxp3*$^{YFP-Cre}$ (n = 5) mice. Data in B, C and E are given as mean ± s.d., and were analyzed with two-tailed t-tests. Each cell type was analyzed individually, without assuming a constant s.d. (*P < 0.05, **P < 0.01, ***P < 0.001, ****P < 0.0001). All data points on graphs represent individual mice isolated and analyzed on at least two different days.

Transfer of SDHA-deficient Treg cells to *Rag1*$^{-/-}$ mice induced a scurfy-like phenotype.

The significant secretions of IFN-γ and IL-4 in SDHA-deficient Treg cells suggest that these Treg cells are inflammatory rather than suppressive in function. To evaluate the inflammatory capacity of SDHA-deficient Treg cells, I adoptively transferred SDHA-deficient Treg cells and wild-type Treg cells to *Rag1*$^{-/-}$ mice. At 8 weeks after transfer, mice were sacrificed and evaluated. SDHA-deficient Treg-cell-transferred Rag1$^{-/-}$ mice showed some skin lesions and scales on the face. HE slides showed that inflammatory cell infiltration was elevated especially in the skin of SDHA-deficient Treg-cell-transferred *Rag1*$^{-/-}$ mice as compared to that in wild-type Treg-cell-transferred *Rag1*$^{-/-}$ mice (Figure 8A). Total immune cell counts of peripheral lymphoid organs tended to be higher in SDHA-deficient Treg-cell-transferred *Rag1*$^{-/-}$ mice than in wild-type Treg-cell-transferred *Rag1*$^{-/-}$ mice (Figure 8B). Moreover, higher inflammatory cytokine production, especially IFN-γ, was observed from SDHA-deficient Treg cells as compared to wild-type Treg cells (Figure 8C). SDHA-deficient Treg-cell-transferred *Rag1*$^{-/-}$ mice showed a lower ratio of Treg cells/CD4^{+} T cells and lower FOXP3 expression on Treg cells as compared to those in wild-type Treg-cell-transferred *Rag1*$^{-/-}$ mice (Figure 8D). These

findings indicate that SDHA-deficient Treg cells not only lose their suppressive capacity, but also gain inflammatory capacity.

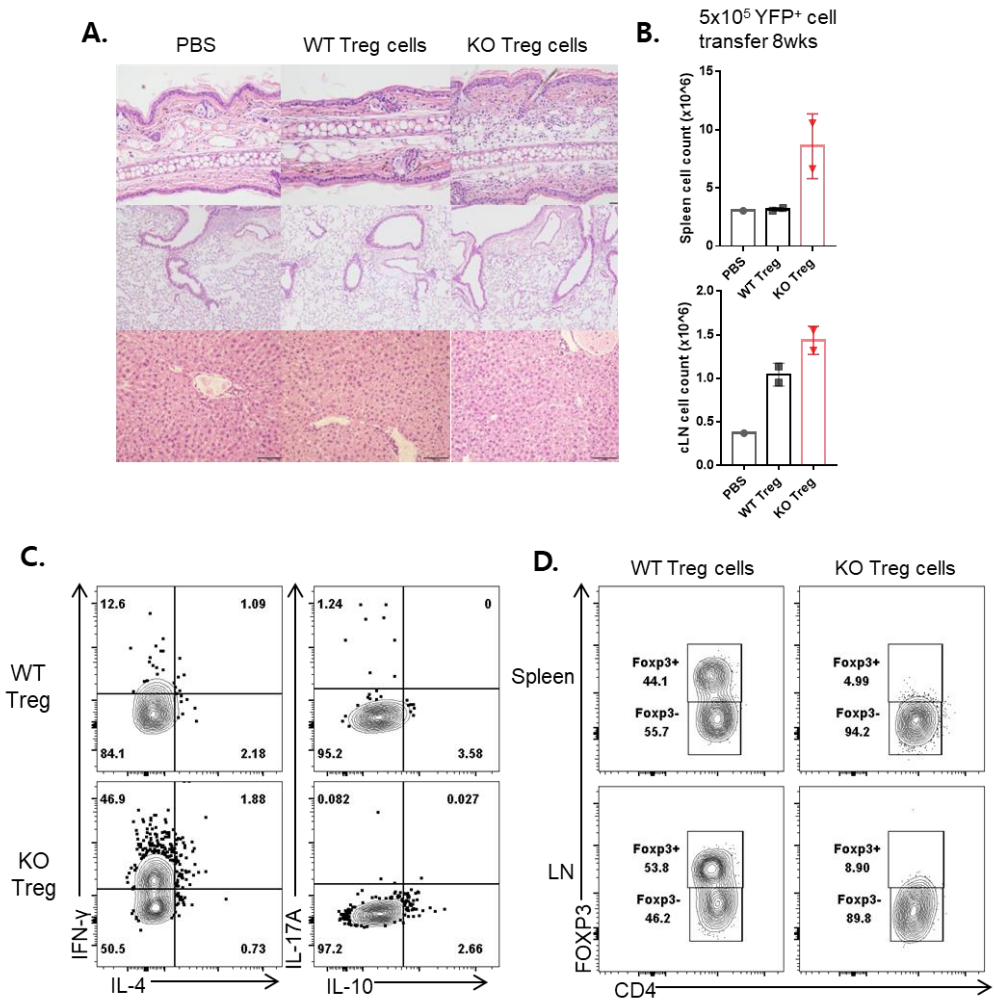

Figure 8. Transfer of SDHA-deficient Treg cells to *Rag1*$^{-/-}$ mice induced s scurfy-like phenotype. 5x10^5 Treg cells from wild-type (n = 2) and *Sdha*$^{fl/fl}$*Foxp3*$^{YFP-Cre}$ (n = 2) mice were injected into the tail veins of *Rag1*$^{-/-}$ mice. A *Rag1*$^{-/-}$ mouse injected with PBS was used as control (n = 1). **A.** Representative images of skin, lung, and liver tissues of *Rag1*$^{-/-}$ mice. **B.** Total cell numbers of spleen and lymph nodes in *Rag1*$^{-/-}$ mice

injected with PBS, wild-type Treg cells, and SDHA-deficient (KO) Treg cells. **C.** Cytokine production from wild-type (WT) Treg cells and KO Treg cells. **D.** FOXP3 expression in Treg cells from WT and KO Treg-cell-transferred *Rag1*$^{-/-}$ mice.

Increased cytokine production from SDHA-deficient Treg cells was partly due to increased glycolysis.

SDHA is one of the key molecules in OXPHOS, and therefore, metabolic reprogramming might occur in order to compensate for defective OXPHOS in *Sdha*$^{fl/fl}$*Foxp3*$^{YFP-Cre}$ mice. To explore metabolic reprogramming in SDHA-deficient Treg cells, targeted metabolic profiling by GC-MS/MS was performed. Among the metabolites analyzed, succinate was heavily accumulated and metabolites related to glycolysis tended to be elevated in SDHA-deficient Treg cells, as compared to wild-type Treg cells (Figure 9). Moreover, mRNA expressions of glycolysis-related genes, such as *HK2*, *PFKM*, and *LDHA*, were elevated in SDHA-deficient Treg cells relative to wild-type Treg cells (Figure 10A). These findings suggest that glycolysis might be elevated in SDHA-deficient Treg cells.

It was previously noted that glycolysis plays a key role in the effector function of conventional T cells. Therefore, I evaluated the effects of elevated glycolysis in SDHA-deficient Treg cells. When glycolysis was shut down by 2-Deoxy-D-glycose (2-DG), the elevated inflammatory cytokine secretion from SDHA-deficient Treg cells decreased but was not completely normalized to the levels observed in wild-type Treg cells (Figure 10B). Therefore, increased inflammatory cytokine secretion in

SDHA-deficient Treg cells was partly due to the increased glycolysis.

In addition to the effect of glycolysis, further research will be needed to elucidate the effect of marked accumulation of succinate or otherwise altered metabolic pathways on Treg cells.

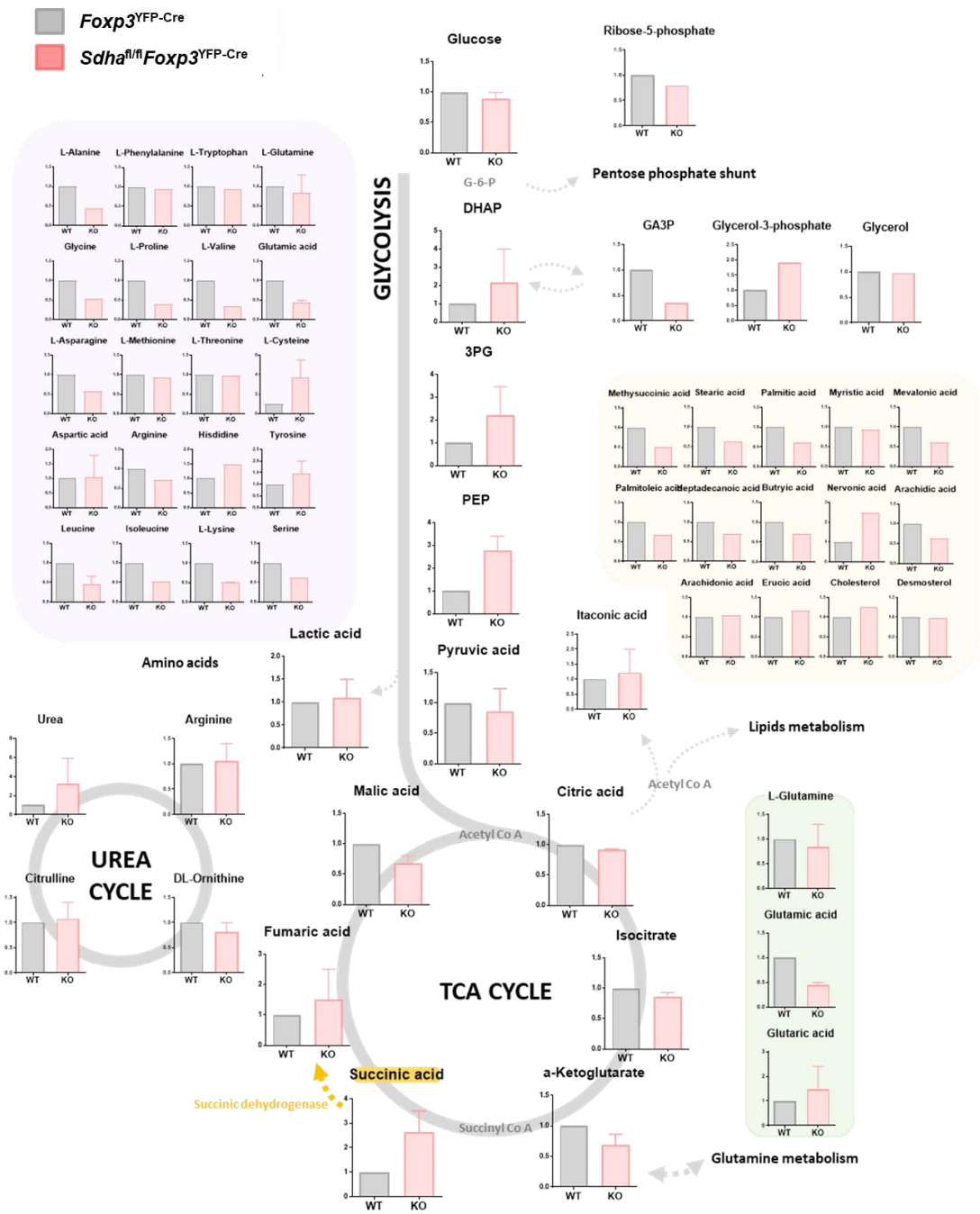

Figure 9. Targeted metabolic profiling by GC-MS/MS. Fold changes of metabolites in Treg cells from wild-type (n = 2) and *Sdha*$^{fl/fl}$*Foxp3*$^{YFP-Cre}$

(n = 2) mice. More than $1x10^6$ cells were used in each experiment. Two sets of experiments were performed on two different days.

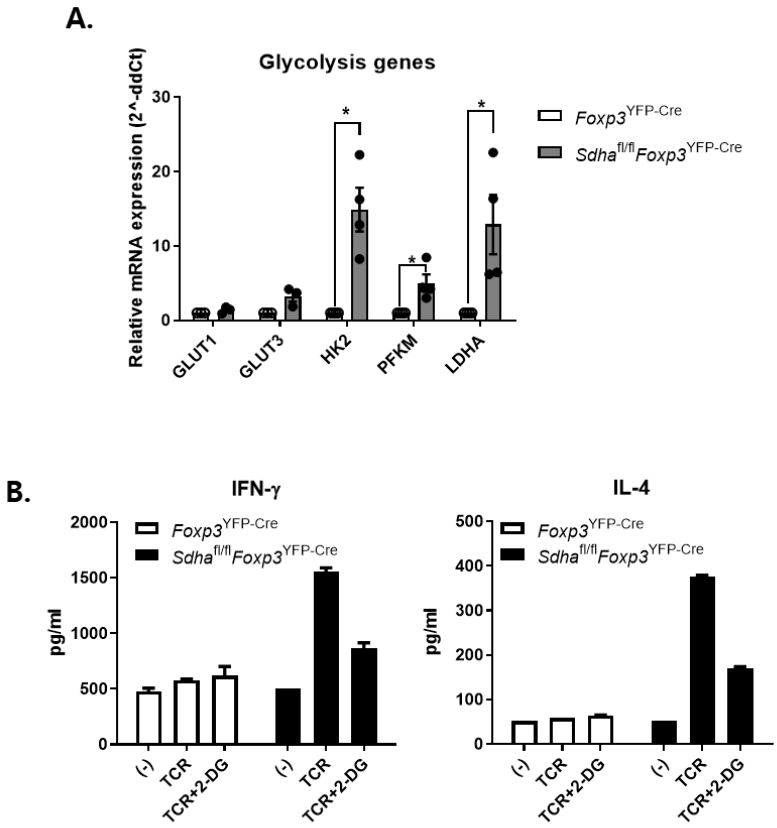

Figure 10. Increased cytokine production in SDHA-deficient Treg cells was partly dependent on increased glycolysis. A. mRNA expression of glycolysis-related genes was analyzed in Treg cells of wild-type (n = 4) and *Sdha*$^{fl/fl}$*Foxp3*$^{YFP-Cre}$ mice (n = 4). **B.** Differential cytokine production after suppression of glycolysis by treatment with 0.5 mM 2-DG was evaluated in Treg cells from wild-type (n = 2) and *Sdha*$^{fl/fl}$*Foxp3*$^{YFP-Cre}$ mice (n = 2). Data are given as mean ± s.d. and were analyzed with two-tailed t-tests without assuming a constant s.d. (*P < 0.05). All data points on graphs represent individual mice isolated and analyzed on at least two different days.

SDHA-deficient Treg cells showed mitochondrial dysfunction.

As previously mentioned, SDHA is one of the key molecules in OXPHOS. Therefore, SDHA deficiency might result in alteration of mitochondrial function. MitoTracker and MitoSOX staining were conducted in order to evaluate mitochondrial function. MitoSOX expression, which is indicative of mitochondrial ROS production, was increased. MitoTracker expression, which is indicative of mitochondrial mass, was not statistically different between SDHA-deficient Treg cells and wild-type Treg cells (Figure 11). Even though there was no decrease in mitochondrial mass, increased mitochondrial ROS production indicated that SDHA-deficient Treg cells might suffer from mitochondrial dysfunction. Further studies will be needed to figure out how to relate mitochondrial dysfunction and the altered integrity/functionality of Treg cells.

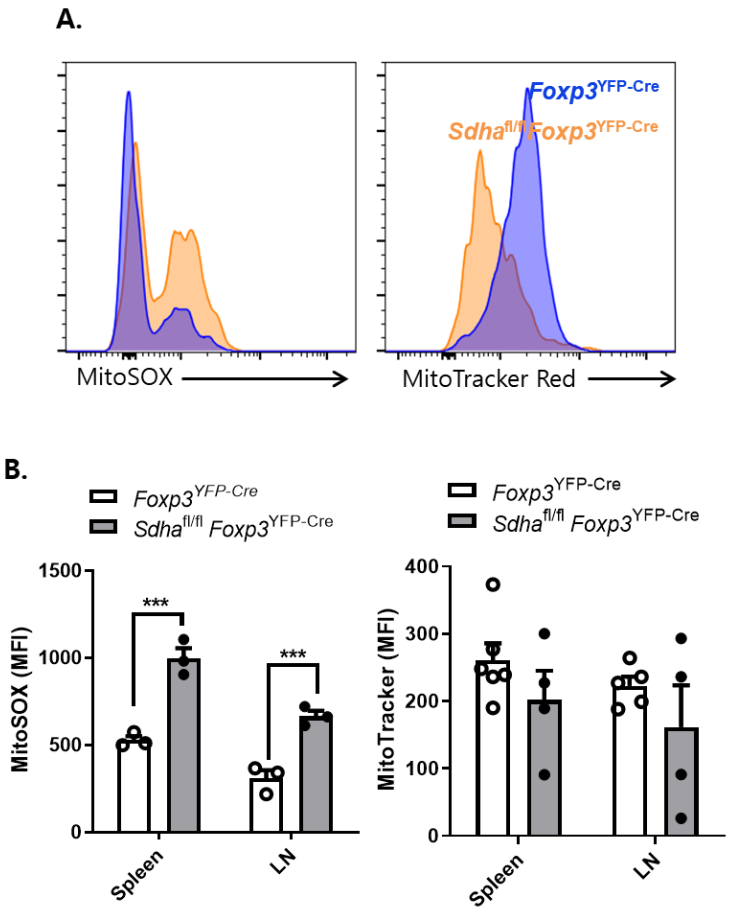

Figure 11. SDHA-deficient Treg cells showed mitochondrial dysfunction. A-B. Mitochondrial ROS and mass evaluated in Treg cells of wild-type (n = 4) and *Sdha*$^{fl/fl}$*Foxp3*-Cre mice (n = 3). Data in B are given as mean ± s.d. and were analyzed with two-tailed t-tests without assuming a constant s.d. (***P < 0.001). All data points on the graphs represent individual mice.

Tumor growth is reduced in *Sdha*$^{fl/fl}$*Foxp3*$^{EGFP-cre-ERT2}$ mice as compared to wild-type mice.

Next, I investigated the suppressive capacity of SDHA-deficient Treg cells in the context of tumor immunity. I established the tumor mouse model by injecting MC38 colon cancer cells into *Sdha*$^{fl/fl}$*Foxp3*$^{EGFP-cre-ERT2}$ (*Sdha* inducible KO, iKO) mice and *Foxp3*$^{EGFP-cre-ERT2}$ (wild-type) mice. To knock out *Sdha*, 100 μL of 20 mg/mL tamoxifen was administered intraperitoneally on days 3, 4, 6, 7, and 8 after tumor inoculation. Tumor growth was limited in iKO mice as compared to that in wild-type mice (Figure 12A-C). Upon immunoprofiling of the tumor tissues, it was found that myeloid cells were not significantly different between the two groups, but the quantities of $CD8^+$ T cells tended to be greater and those of Treg cells were lower in iKO mice than in wild-type mice (Figure 12D-E). FOXP3 expression tended to be lower in iKO mice than in wild-type mice, but the difference was not statistically significant (Figure 12F). Production of IL-17A from $CD4^+$ T cells, $CD8^+$ T cells, and Treg cells was significantly elevated in the iKO mice (Figure 12G-I). Production of IFN-γ from $CD4^+$ T cells and Treg cells was also tended to be elevated in the iKO mice (Figure 12G-I).

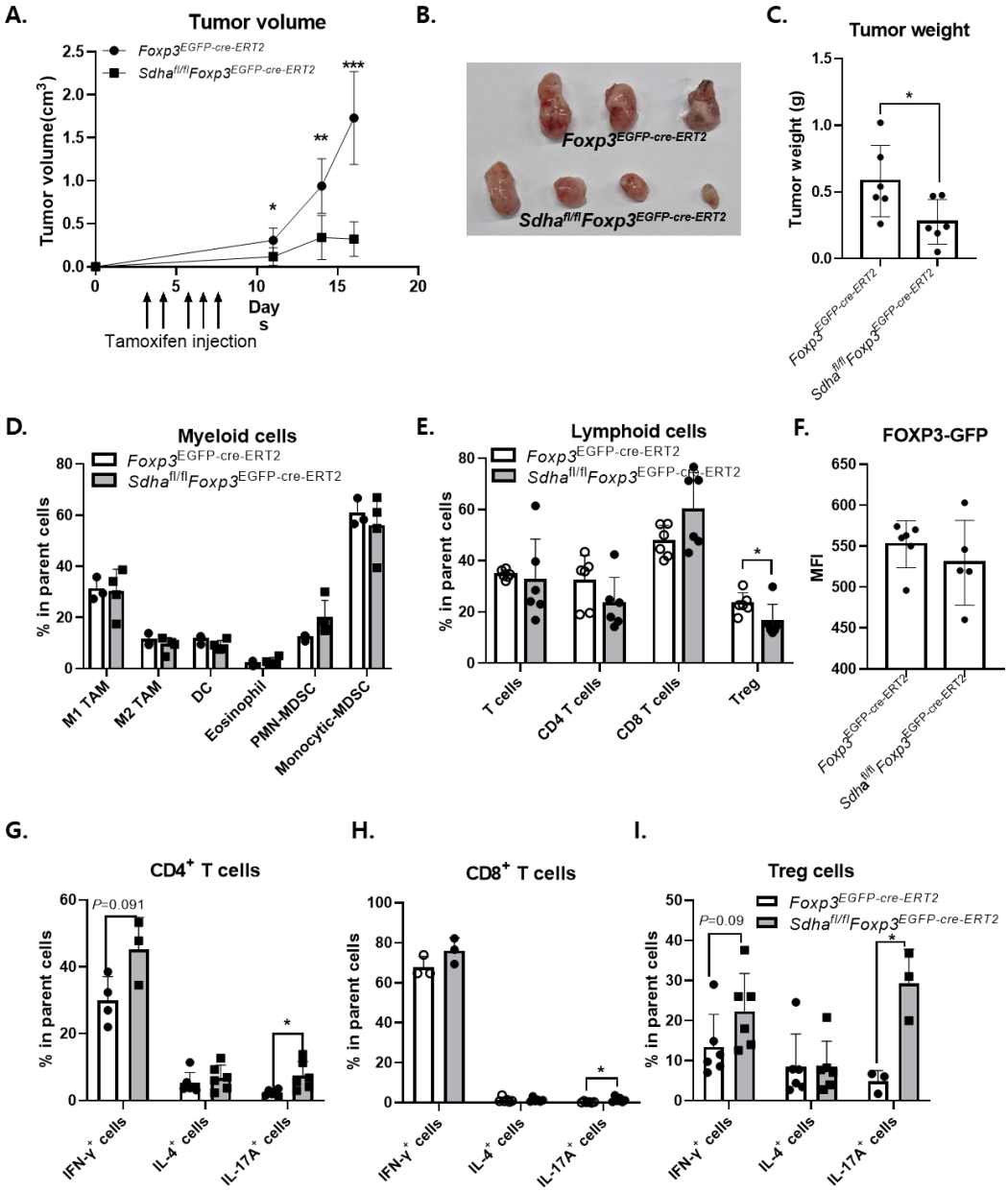

Figure 12. Tumor growth is reduced in *Sdha*$^{fl/fl}$*Foxp3*$^{EGFP-cre-ERT2}$ mice compared to wild-type mice. 5x10^5 MC38 cells were injected into the flanks of wild-type (*Foxp3*$^{EGFP-cre-ERT2}$, n = 6) and SDHA iKO (*Sdha*$^{fl/fl}$*Foxp3*$^{EGFP-cre-ERT2}$, n = 6) mice. Tamoxifen was administered on

days 3, 4, 6, 7, and 8 after tumor injection. **A.** Growth of MC38 colon cancer cells in wild-type and SDHA iKO mice. **B.** Representative images of tumors from wild-type and SDHA iKO mice. **C.** Tumor weights from wild-type and SDHA iKO mice. **D-E.** Myeloid and lymphoid cell infiltration in tumor tissues. **F.** FOXP3 expression in tumor-infiltrating Treg cells. **G-I.** Percentages of cytokine-producing $CD4^+$ T cells, $CD8^+$ T cells, and Treg cells from tumor tissues. Data in **A** and **C-I** are given as mean ± s.d. and were analyzed with two-tailed t-tests without assuming a constant s.d. (*$P < 0.05$, **$P < 0.01$, **$P < 0.001$). All data points on the graphs represent individual mice isolated.

Positive correlation between FOXP3 and SDHA expression was also observed in human tumor tissues.

To evaluate the clinical implication of SDHA-deficient Treg cells in the context of human tumors, I attempted to find a distinctive marker for SDHA-deficient Treg cells using single-cell RNAseq data from human lung cancer tissue, but I was unable to find a distinctive marker. However, I did find a positive correlation between SDHA and FOXP3 expression in human tumor tissues. I divided a population of $CD4^{+}$ T cells according to their FOXP3 expression and then analyzed their SDHA expression. In accordance with the findings from the mouse experiments, $FOXP3^{low}$ Treg cells showed lower expression of SDHA than $FOXP3^{high}$ Treg cells in human lung cancers and colon cancers (Figure 13). Even though the correlation is not perfect, $FOXP3^{low}$ Treg cells might be able to serve as a proxy for SDHA-deficient Treg cells in human tumor tissue models.

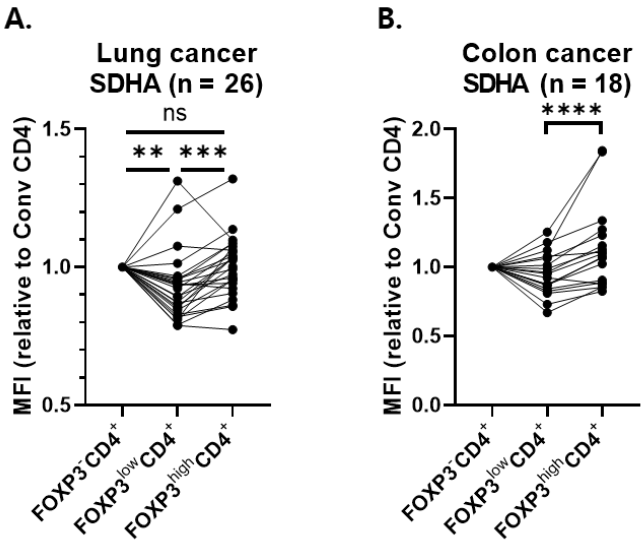

Figure 13. A positive correlation between FOXP3 and SDHA expression was also identified in human tumor tissues. A. SDHA expression on conventional $CD4^+$ T cells, $FOXP3^{low}$ Treg cells, and $FOXP3^{high}$ Treg cells in lung cancer tissues (n=26). **B.** SDHA expression on conventional $CD4^+$ T cells, $FOXP3^{low}$ Treg cells, and $FOXP3^{high}$ Treg cells in lung cancer tissues (n=18). Data were analyzed with one-way ANOVA with a Tukey test for multiple comparisons (**$P < 0.01$, ***$P < 0.001$, ****$P < 0.0001$). All data points on the graphs represent individual cases.

FOXP3^{low} Treg cells showed increased proinflammatory cytokine secretion in human lung cancer tissues

I divided a subpopulation of Treg cells according to FOXP3 and CD45RA expression (Figure 14A), and evaluated cytokine production from each subpopulation of Treg cells. The composition of the Treg cell subpopulation differed among cases. Some cases showed high infiltration of CD45RA^{-}FOXP3^{low}CD4^{+} T cells, and others did not (Figure 14A). As in the mouse models, CD45RA^{-}FOXP3^{low}CD4^{+} T cells secreted more inflammatory cytokines, such as IFN-γ and IL-17A, than CD45RA^{-}FOXP3^{high}CD4^{+} T cells. These findings were observed in both of lung ADC and SqCC (Figure 14B-C).

A. Representative images of flow cytometry

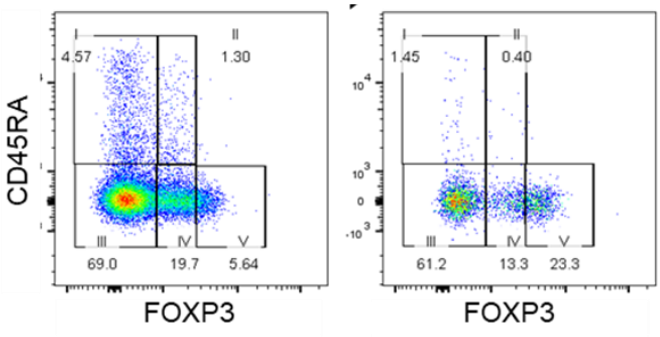

B. Lung squamous cell carcinoma

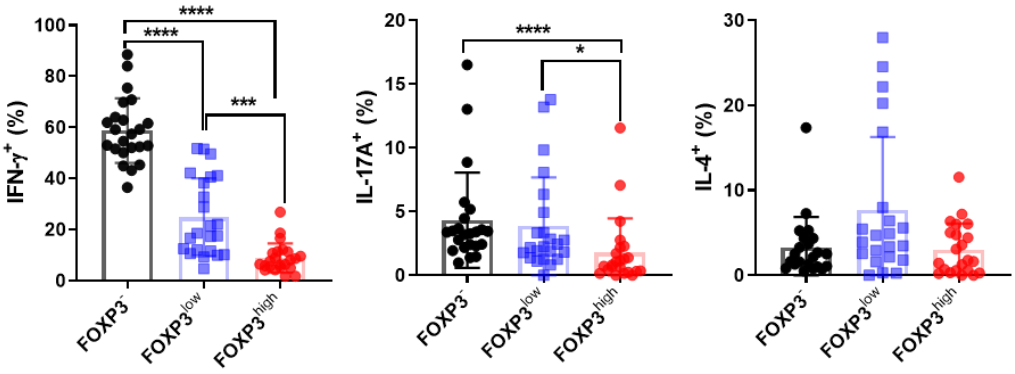

C. Lung adenocarcinoma

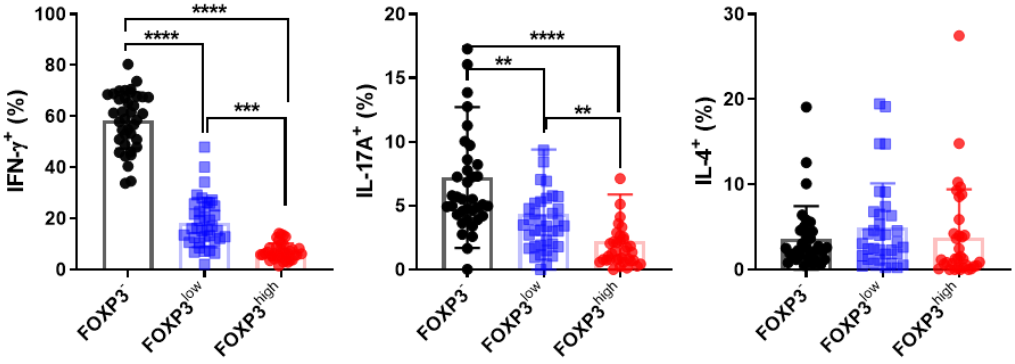

Figure 14. FOXP3^{low} Treg cells showed increased proinflammatory cytokine secretion in human lung cancer tissues. A. Representative images of flow cytometry for subgrouping of Treg cells. High CD45RA^{-}FOXP3^{low}CD4^{+} T cells (left) and low CD45RA^{-}FOXP3^{low}CD4^{+} T cells (right). Percentage of IFN-γ-, IL-17A-, and IL-4-secreting CD45RA^{-}FOXP3^{-}CD4^{+} T cells, CD45RA^{-}FOXP3^{low}CD4^{+} T cells, and CD45RA^{-}FOXP3^{high}CD4^{+} T cells in lung SqCC tissues (**B.** n = 25) and lung ADC tissues (**C.** n = 38). Data are given as mean ± s.d. and were analyzed with Mann-Whitney U-tests with a Dunn test for multiple comparisons (*P < 0.05, **P < 0.01, ***P < 0.001, ****P < 0.0001). All data points on the graphs represent individual cases.

Prognosis is better for patients with high FOXP3^{low} cell infiltration compared to patients with poor FOXP3^{low} cell infiltration

To evaluate the potential clinical implications of FOXP3^{low} Treg cell populations, I evaluated CD8 and FOXP3-immunostained slides using an image analyzer (Figure 15A). Survival analysis was conducted for lung SqCC and colon ADC. As expected, the FOXP3^{low} cell/FOXP3^{+} cell ratio was a good prognostic marker for overall survival. In advanced stage (≥ pT3) of lung SqCC and colon ADC cases, patients with higher FOXP3^{low} cell/FOXP3^{+} cell ratios showed better overall survival (OS) (lung SqCC, P =0.001; colon ADC, P = 0.009). Moreover, the ratio of FOXP3^{low}/FOXP3^{+} cells had better prognostic power than CD8^{+} T cell infiltration, especially in advanced tumors (Figure 15B-C).

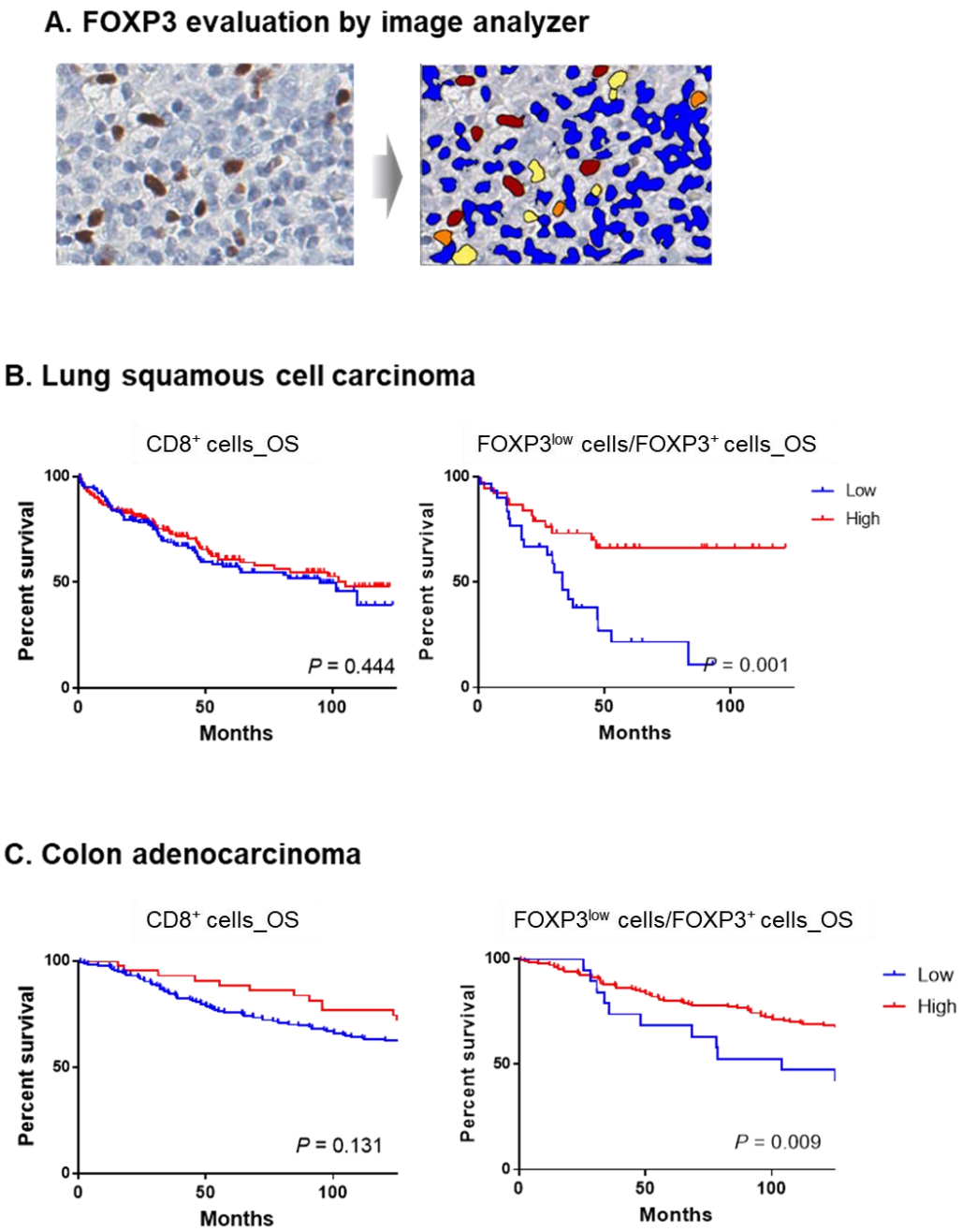

Figure 15. Prognosis is better for patients with high FOXP3^{low} cell infiltration compared to patients with poor FOXP3^{low} cell infiltration. A.

Representative image of FOXP3 stained lung SqCC tissue and corresponding image of automatically analyzed FOXP3 expression by the image analyzer. Brown and orange denote $FOXP3^{high}$ cells, yellow denotes $FOXP3^{low}$ cells, and blue denotes $FOXP3^{negative}$ cells. **B.** Overall survival according to $CD8^{+}$ cell infiltration and ratio of $FOXP3^{low}$ cells/$FOXP3^{+}$ cells in ≥ 5 cm (pT3) lung SqCC (n = 68). **C.** Overall survival according to $CD8^{+}$ cell infiltration and ratio of $FOXP3^{low}$ cells/$FOXP3^{+}$ cells in ≥ pT3 and microsatellite stable (MSS) colon ADC (n = 187). Survival analysis was done using Kaplan−Meier and Log rank tests.

Abundant FOXP3^{low} cell infiltration tended to correlate to better response and overall survival in lung SqCC patients with PD-1/PD-L1 blockades.

To evaluate the clinical implications of FOXP3^{low} Treg cell infiltration in patients undergoing immunotherapy, survival analysis was done in lung SqCC subjected to PD-1/PD-L1 blockades. Patients with high FOXP3^{low} cell infiltration tended to respond better to PD-1/PD-L1 blockades (Figure 16A) and had better OS (Figure 16B-C) as compared to those with low FOXP3^{low} cell infiltration. Progression-free survival did not differ according to the level of FOXP3^{low} cell infiltration. There was no statistical significance found in this analysis, which might be because of the small number of patients studied, and therefore further validation with a larger cohort is needed to clarify these findings.

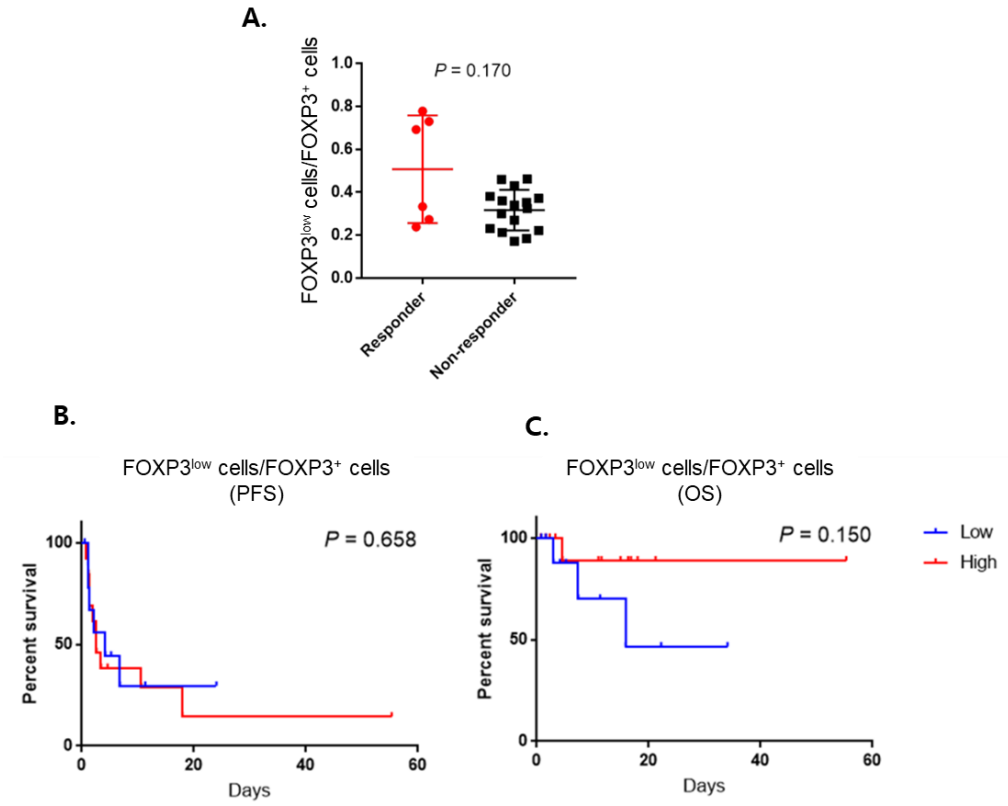

Figure 16. Prognostic power of FOXP3^{low} cell infiltration in lung SqCC patients undergoing PD-1/PD-L1 blockade therapy. A. Ratio of FOXP3^{low}/FOXP3^{+} cells according to response to PD-1/PD-L1 blockades. **B-C.** Differences in progression free survival and overall survival according to the ratio of FOXP3^{low} cells/FOXP3^{+} cells. Data in A is given as mean ± s.d. and was analyzed with two-tailed t-tests without assuming a constant s.d. Survival analysis was done using Kaplan-Meier and Log rank tests.

DISCUSSION

In this study, I found that mice with SDHA-deficient Treg cells exhibited a scurfy phenotype early in life. The proportion of Treg cells to $CD4^+$ T cells and the suppressive capacity of the Treg cells were markedly decreased in SDHA-deficient Treg cells as compared to wild-type Treg cells. On the other hand, SDHA-deficient Treg cells gained an inflammatory function via increased secretion of inflammation cytokines such as IFN-γ and IL-4. This inflammatory phenotype was partly resultant from increased glycolysis. SDHA-deficient Treg cells showed lower FOXP3 expression than wild-type Treg cells. This positive correlation between FOXP3 and SHDA was also identified in human tumor tissues. Therefore, $FOXP3^{low}$ Treg cells might be able to partially represent SDHA-deficient Treg cells in human tumor models. Higher infiltration of $FOXP3^{low}$ Treg cells implied better survival for patients undergoing conventional therapies or immunotherapies. Therefore, our findings confirm the essential role of SDHA in Treg cells. Previously, a few patients with germline mutations in the SDH family were reported to have autoimmune diseases (22). The aforementioned findings might partially explain such clinical manifestations.

The results of this study emphasize the essential role of SDHA in maintaining the stability of Treg cells. A previous study also reported that

alterations to metabolic pathways or metabolism-related genes can result in altered Treg stability and functioning (18, 28-30). For example, inhibition of glycolysis or deletion of *mTOR*, upstream of HIF-1α promotes Treg cell generation and stability (31-35). On the contrary, increased glycolysis due to upregulation of HIF-1α was capable of decreasing FOXP3 expression via ubiquitination and proteasomal degradation (31, 36). In addition, it has been reported that increased lipid metabolism contributed to stability and functional maturation of Treg cells (34, 35). In regard to accumulated metabolites, previous studies have reported that accumulation of succinate and 2-hydroxyglutarate (2-HG) in Treg cells drove the downregulation of expression of suppressive genes such as *PD-1, CD73, TIGIT*, and *NRP1* (37, 38). Similar to the results of the present study, Weinberg et al. reported that mitochondrial complex III is essential for the suppressive function of Treg cells (37). Loss of complex III in Treg cells led to decreased suppressive capacity without altering proliferation capacity and survival. Complex-III-deficient Treg cells also showed stable FOXP3 expression. In contrast, in our study, the loss of SDHA, which is a component of complex II, resulted in impaired suppressive function alongside lower numbers of Treg cells and lower FOXP3 expression. These differences might partly derive from the differential metabolite profiles. A previous paper reported that Antimycin

A (a complex III inhibitor) increased the levels of both succinate and 2-HG, but 3-nitropropionic acid (3-NPA, a complex II inhibitor) increased the level of succinate only. The authors suggested that inhibition of different respiratory complexes results in differential metabolite concentrations, thereby provoking distinct changes in gene expression (37). In this study, I also identified an increased level of succinate resulting from SDHA deficiency, but I was unable to evaluate levels of 2-HG. Further detailed studies are needed to elucidate what caused these differences.

The gained inflammatory phenotype of SDHA-deficient Treg cells observed in this study can be partly explained by increased glycolysis. Although the detailed mechanism was not elucidated in this study, increased glycolysis might repress FOXP3 expression via the non-glycolytic activity of enolase-1, an enzyme involved in glycolysis (39). Additionally, accumulation of succinate may play a role in the development of this phenotype. A previous paper reported that succinate induced secretion of inflammatory cytokines (such as IL-1β) in macrophages by stabilizing HIF-1α (40). Moreover, HIF-1α is a key regulator of glycolysis, especially under hypoxic conditions. Further studies will be needed to find out whether or not succinate plays a similar role in Treg cells as it does in macrophages.

As a result of SDHA deficiency, a large number of FOXP3^{low} Treg cells were induced. I found that with the loss of eTreg (FOXP3^{high} Treg cell) cells, increased quantities of FOXP3^{low} Treg cells conferred scurfy phenotypes and marked anti-tumor immunity in mouse tumor models. Moreover, I observed a positive correlation between SDHA and FOXP3 expression on Treg cells in human tumors, similar to in the mouse model. Although I did not identify a solid causal relationship between SDHA and FOXP3, FOXP3 expression was well matched to cellular SDHA expression. FOXP3^{low} Treg cells in human tumor tissues also showed increased inflammatory cytokine secretion. Therefore, even though the correlation is not perfect, it is possible that FOXP3^{low} Treg cells could be used to represent SDHA-deficient Treg cells in human tumor tissue models.

Although Saito et al. previously suggested the potential prognostic power of FOXP3^{low} Treg cell populations (10), they did not directly compare the difference in survival according to the degree of FOXP3^{low} Treg cell infiltration. Instead, they identified inflammatory phenotypes of FOXP3^{low} Treg cells and then focused on revealing the conditions that induced FOXP3^{low} Treg cell differentiation. They showed that patients with conditions favoring FOXP3^{low} Treg cell differentiation showed better prognosis than others. In this study, I first demonstrated a direct

correlation between expected patient survival and FOXP3^{low} Treg cell infiltration. Previously inconsistent results about the prognostic impacts of Treg cell infiltration might be due to heterogeneity in the Treg subpopulation. Therefore, a more subtle and thorough evaluation of Treg cell infiltration is needed for enabling prediction of patient survival. Further studies elucidating the conditions or factors which favor FOXP3^{low} Treg cell infiltration in various tumor tissues are needed for accurately forecasting patient survival and finding new therapeutic targets.

In summary, our results indicate that SDHA-mediated mitochondrial metabolism is crucial for peripheral homeostasis and tolerance, and that evaluating the abundance and composition of Treg cell subpopulations in TMEs is important for forecasting prognosis.

REFERENCE

1. Sakaguchi S, Yamaguchi T, Nomura T, Ono M. Regulatory T Cells and Immune Tolerance. Cell. 2008;133(5):775-87.

2. Fontenot JD, Gavin MA, Rudensky AY. Foxp3 programs the development and function of CD4+CD25+ regulatory T cells. Nature immunology. 2003;4(4):330-6.

3. Hori S, Nomura T, Sakaguchi S. Control of regulatory T cell development by the transcription factor Foxp3. Science (New York, NY). 2003;299(5609):1057-61.

4. Khattri R, Cox T, Yasayko SA, Ramsdell F. An essential role for Scurfin in CD4+CD25+ T regulatory cells. Nature immunology. 2003;4(4):337-42.

5. Brunkow ME, Jeffery EW, Hjerrild KA, Paeper B, Clark LB, Yasayko SA, et al. Disruption of a new forkhead/winged-helix protein, scurfin, results in the fatal lymphoproliferative disorder of the scurfy mouse. Nature genetics. 2001;27(1):68-73.

6. Bennett CL, Christie J, Ramsdell F, Brunkow ME, Ferguson PJ, Whitesell L, et al. The immune dysregulation, polyendocrinopathy, enteropathy, X-linked syndrome (IPEX) is caused by mutations of FOXP3. Nature genetics. 2001;27(1):20-1.

7. Yan B, Xiong J, Ye Q, Xue T, Xiang J, Xu M, et al. Correlation and

prognostic implications of intratumor and tumor draining lymph node Foxp3(+) T regulatory cells in colorectal cancer. BMC gastroenterology. 2022;22(1):122.

8. Idos GE, Kwok J, Bonthala N, Kysh L, Gruber SB, Qu C. The Prognostic Implications of Tumor Infiltrating Lymphocytes in Colorectal Cancer: A Systematic Review and Meta-Analysis. Scientific Reports. 2020;10(1):3360.

9. Miyara M, Yoshioka Y, Kitoh A, Shima T, Wing K, Niwa A, et al. Functional delineation and differentiation dynamics of human CD4+ T cells expressing the FoxP3 transcription factor. Immunity. 2009;30(6):899-911.

10. Saito T, Nishikawa H, Wada H, Nagano Y, Sugiyama D, Atarashi K, et al. Two FOXP3+CD4+ T cell subpopulations distinctly control the prognosis of colorectal cancers. Nature Medicine. 2016;22(6):679-84.

11. Guerra L, Bonetti L, Brenner D. Metabolic Modulation of Immunity: A New Concept in Cancer Immunotherapy. Cell Rep. 2020;32(1):107848.

12. Leone RD, Powell JD. Metabolism of immune cells in cancer. Nature Reviews Cancer. 2020;20(9):516-31.

13. Gerriets VA, Kishton RJ, Nichols AG, Macintyre AN, Inoue M, Ilkayeva O, et al. Metabolic programming and PDHK1 control CD4+ T cell

subsets and inflammation. The Journal of clinical investigation. 2015;125(1):194-207.

14. Michalek RD, Gerriets VA, Jacobs SR, Macintyre AN, MacIver NJ, Mason EF, et al. Cutting edge: distinct glycolytic and lipid oxidative metabolic programs are essential for effector and regulatory CD4+ T cell subsets. J Immunol. 2011;186(6):3299-303.

15. Viola A, Munari F, Sánchez-Rodríguez R, Scolaro T, Castegna A. The Metabolic Signature of Macrophage Responses. Front Immunol. 2019;10:1462.

16. Angelin A, Gil-de-Gómez L, Dahiya S, Jiao J, Guo L, Levine MH, et al. Foxp3 Reprograms T Cell Metabolism to Function in Low-Glucose, High-Lactate Environments. Cell Metab. 2017;25(6):1282-93.e7.

17. Gerriets VA, Kishton RJ, Johnson MO, Cohen S, Siska PJ, Nichols AG, et al. Foxp3 and Toll-like receptor signaling balance Treg cell anabolic metabolism for suppression. Nature Immunology. 2016;17(12):1459-66.

18. Kurniawan H, Franchina DG, Guerra L, Bonetti L, Baguet LS, Grusdat M, et al. Glutathione Restricts Serine Metabolism to Preserve Regulatory T Cell Function. Cell metabolism. 2020;31(5):920-36.e7.

19. Rustin P, Munnich A, Rötig A. Succinate dehydrogenase and human diseases: new insights into a well-known enzyme. European

Journal of Human Genetics. 2002;10(5):289-91.

20. Baysal BE, Rubinstein WS, Taschner PE. Phenotypic dichotomy in mitochondrial complex II genetic disorders. Journal of Molecular Medicine. 2001;79(9):495-503.

21. Sun F, Huo X, Zhai Y, Wang A, Xu J, Su D, et al. Crystal structure of mitochondrial respiratory membrane protein complex II. Cell. 2005;121(7):1043-57.

22. Jha A, de Luna K, Balili CA, Millo C, Paraiso CA, Ling A, et al. Clinical, Diagnostic, and Treatment Characteristics of SDHA-Related Metastatic Pheochromocytoma and Paraganglioma. Front Oncol. 2019;9:53.

23. Amin MBESBAJCoC. AJCC cancer staging manual2017.

24. Edge SB. AJCC Cancer Staging Manual. New York, N.Y.: Springer; 2011.

25. Faubert B, Vincent EE, Griss T, Samborska B, Izreig S, Svensson RU, et al. Loss of the tumor suppressor LKB1 promotes metabolic reprogramming of cancer cells via HIF-1α. Proc Natl Acad Sci U S A. 2014;111(7):2554-9.

26. Mamer O, Gravel SP, Choinière L, Chénard V, St-Pierre J, Avizonis D. The complete targeted profile of the organic acid intermediates of the citric acid cycle using a single stable isotope dilution

analysis, sodium borodeuteride reduction and selected ion monitoring GC/MS. Metabolomics. 2013;9(5):1019-30.

27. Kempkes RWM, Joosten I, Koenen HJPM, He X. Metabolic Pathways Involved in Regulatory T Cell Functionality. Frontiers in Immunology. 2019;10.

28. Timilshina M, You Z, Lacher SM, Acharya S, Jiang L, Kang Y, et al. Activation of Mevalonate Pathway via LKB1 Is Essential for Stability of T(reg) Cells. Cell Rep. 2019;27(10):2948-61.e7.

29. Yan Y, Huang L, Liu Y, Yi M, Chu Q, Jiao D, et al. Metabolic profiles of regulatory T cells and their adaptations to the tumor microenvironment: implications for antitumor immunity. J Hematol Oncol. 2022;15(1):104.

30. Wang H, Franco F, Tsui YC, Xie X, Trefny MP, Zappasodi R, et al. CD36-mediated metabolic adaptation supports regulatory T cell survival and function in tumors. Nature immunology. 2020;21(3):298-308.

31. Shi LZ, Wang R, Huang G, Vogel P, Neale G, Green DR, et al. HIF1α-dependent glycolytic pathway orchestrates a metabolic checkpoint for the differentiation of TH17 and Treg cells. Journal of Experimental Medicine. 2011;208(7):1367-76.

32. Delgoffe GM, Kole TP, Zheng Y, Zarek PE, Matthews KL, Xiao B, et al. The mTOR Kinase Differentially Regulates Effector and Regulatory

T Cell Lineage Commitment. Immunity. 2009;30(6):832-44.

33. Cheng SC, Quintin J, Cramer RA, Shepardson KM, Saeed S, Kumar V, et al. mTOR- and HIF-1α-mediated aerobic glycolysis as metabolic basis for trained immunity. Science (New York, NY). 2014;345(6204):1250684.

34. Wang H, Franco F, Tsui Y-C, Xie X, Trefny MP, Zappasodi R, et al. CD36-mediated metabolic adaptation supports regulatory T cell survival and function in tumors. Nature Immunology. 2020;21(3):298-308.

35. Lim SA, Wei J, Nguyen T-LM, Shi H, Su W, Palacios G, et al. Lipid signalling enforces functional specialization of Treg cells in tumours. Nature. 2021;591(7849):306-11.

36. Dang EV, Barbi J, Yang HY, Jinasena D, Yu H, Zheng Y, et al. Control of T(H)17/T(reg) balance by hypoxia-inducible factor 1. Cell. 2011;146(5):772-84.

37. Weinberg SE, Singer BD, Steinert EM, Martinez CA, Mehta MM, Martínez-Reyes I, et al. Mitochondrial complex III is essential for suppressive function of regulatory T cells. Nature. 2019;565(7740):495-9.

38. Lu C, Thompson Craig B. Metabolic Regulation of Epigenetics. Cell Metabolism. 2012;16(1):9-17.

39. De Rosa V, Galgani M, Porcellini A, Colamatteo A, Santopaolo M, Zuchegna C, et al. Glycolysis controls the induction of human regulatory T cells by modulating the expression of FOXP3 exon 2 splicing variants. Nature immunology. 2015;16(11):1174-84.

40. Tannahill GM, Curtis AM, Adamik J, Palsson-McDermott EM, McGettrick AF, Goel G, et al. Succinate is an inflammatory signal that induces IL-1β through HIF-1α. Nature. 2013;496(7444):238-42.

초 록

조절 T 세포에서 숙신산 탈수소효소의 기능

김세희

의학과

병리학 전공

서울대학교 대학원

조절 T 세포는 말초 면역 조절 및 다양한 면역치료의 중요 조절인자로 여겨지기에, 이 세포에 대한 관심이 늘고 있다. 이 세포의 생리에 대한 연구 중, 조절 T 세포 고유의 대사 프로그램이 다양하게 연구되었으나, 아직까지도 대사 프로그램 조절에 따른 임상적 의미 및 암 조직에서의 치료표적으로써의 활용에 대해서는 잘 알려져 있지 않다. 숙신산 탈수소효소는 미토콘드리아 대사의 주요 인자 중 하나로, 시트르산 회로와 전자전달계 둘 다에 관여하고 있다. 이번 연구에서 우리는 숙신산 탈수소효소의 아형인 숙신산 탈수소효소A를 조절 T 세포에서 결핍시킴으로써, 이 효소가 조절 T 세포의 항상성 및 면역 억제 기능에 미치는 영향을 연구하였다. 아형인 숙신산 탈수소효소A가 조절 T 세포에서 결핍되면 면역 억제 기능이 저하되고, 전신 자가면역 질환이 야기되었다. 아형인 숙신산 탈수소효소A 결핍 조절 T 세포는 염증성 싸이토카인의 분비가 증가되고, FOXP3 발현이 저하된다. 이러한 변화는 부분적으로 상대적으로 증가한 해당작용에서 기인한 것으로

확인되었다. 이 마우스 모델에서 종양의 발생 및 성장은 대조군에 비해 현저히 저하되었다. 마우스 모델의 숙신산 탈수소효소A 결핍 조절 T 세포와 유사하게, 인간 종양 조직 내 FOXP3 저발현 조절 T 세포는 FOXP3 고발현 조절 T 세포보다 상대적으로 염증성 사이토카인의 분비가 증가되어 있었다. 따라서 FOXP3 저발현 조절 T 세포/ 조절 T 세포 비율이 높은 경우 환자의 예후가 좋음을 고식적 치료를 받은 폐 편평세포암 및 결장암에서 확인하였다. 이러한 경향은 PD-1/PD-L1 면역치료를 받은 환자군에서도 확인되었다. 결론적으로 숙신산 탈수소효소는 조절 T 세포의 유지 및 면역 억제 기능에 중요하며, 종양 조직에서 FOXP3 발현에 따른 조절 T 세포의 아형을 평가하는 것을 환자의 예후를 예측하는데 중요하다.

주요어: 숙신산 탈수소효소, 미토콘드리아 대사, FOXP3, 조절 T 세포, 종양

학 번: 2014-30592